Spring 2024

Hysplit in Simulating the Atmospheric Dispersion of Hazardous Aerosols: A Case Study in St. Louis, Missouri

Ahmet Tolga Odabasi
Missouri University of Science and Technology

Department:

HYSPLIT IN SIMULATING THE ATMOSPHERIC DISPERSION OF HAZARDOUS AEROSOLS: A CASE STUDY IN ST. LOUIS, MISSOURI

by

AHMET TOLGA ODABAŞI

A THESIS

Presented to the Graduate Faculty of the

MISSOURI UNIVERSITY OF SCIENCE AND TECHNOLOGY

In Partial Fulfillment of the Requirements for the Degree

MASTER OF SCIENCE

IN

ENVIRONMENTAL ENGINEERING

2023

Approved by:

Yang Wang, Advisor
Shoaib Usman
Hüseyin Şahiner

ABSTRACT

Atmospheric dispersion and transmission play an important role in the behavior and effects of air pollution. Human health can be adversely affected by air pollution in a variety of ways, both immediately and over time. The Hybrid Single Particle Lagrangian Integrated Trajectory Model (HYSPLIT) modeling program, a computer model and software package, tracks the transport trajectories and distributions of air pollution and various pollutants, including radioactive pollutants, in the atmosphere. It also facilitates research on pollution sources. This study simulated the transport of hazardous aerosols in St. Louis region for the years 2020, 2021, and 2022 using the HYSPLIT modeling program. First, the monthly and seasonal atmospheric transport of St. Louis region was determined using the HYSPLIT program in 2020, 2021, and 2022. It also analyzed the air pollutants observed in St. Louis region in 2020, 2021, and 2022. Then, the dates when hazardous aerosols would be at their highest were determined. Backward and forward trajectories were calculated using the HYSPLIT modeling program, and cluster analyses were performed on pollutants entering the region and pollutants being transported out of the region. As a result of the research, the use of fireworks during Fourth of July celebrations has been linked to an increase in the concentration of $PM_{2.5}$ and SO_2 in the atmosphere.

ACKNOWLEDGMENTS

I express my gratitude to everyone who supported me in completing my program. First, I thank the Ministry of National Education of the Republic of Türkiye for rewarding me with a scholarship during my graduate education at Missouri University of Science and Technology and financing my graduate education. I am grateful to my advisor, Dr. Yang Wang, for his support, patience, advice, and feedback throughout my thesis work. I appreciate to Dr. Shoaib Usman and Dr. Hüseyin Şahiner, as members of my thesis committee, for their insightful criticism and recommendations.

In addition, I offer my special thanks to my parents, İhsan and İlknur Odabaşı, and my brother Kağan for their unwavering financial and moral support.

TABLE OF CONTENTS

Page

LIST OF ILLUSTRATIONS

LIST OF TABLES

NOMENCLATURE

Acronyms	Description
AGL	Above Ground Level.
ALR	Atmospheric Lapse Rate.
AQI	Air Quality Index.
ARL	Air Resources Laboratory.
ATD	Atmospheric Transport and Dispersion.
CO	Carbon Monoxide.
DALR	Dry Adiabatic Lapse Rate.
EPA	Environmental Protection Agency.
ELR	Environmental Lapse Rate.
GDAS	Global Data Assimilation System.
GFS	Global Forecast System.
GLO	Ground-level ozone.
HYSPLIT	Hybrid Single Particle Lagrangian Integrated Trajectory Model.
NAAQS	National Ambient Air Quality Standards.
NO	Nitrogen Oxide.
NO_2	Nitrogen Dioxide.
NOAA	National Oceanic and Atmospheric Administration.
O_3	Ozone.
PAHs	Polycyclic Aromatic Hydrocarbons.
Pb	Lead.

PEP	Population Estimates Program.
PM	Particulate Matter.
$PM_{0.1}$	Particulate matter diameter is 0.1 μm or less.
$PM_{2.5}$	Particulate matter diameter is 2.5 μm or less.
PM_{10}	Particulate matter diameter is 10 μm or less.
ppb	Parts per billion.
ppm	Parts per million.
PSI	The Pollutant Standard Index.
SPVAR	The Cluster Spatial Variance.
TEOM	The tapered element oscillating microbalance.
TSV	Total Spatial Variance.
VOCs	Volatile Organic Compounds.

1. INTRODUCTION

The movement of contaminants in the atmosphere is facilitated by processes of transport, dispersion, and deposition. Transport refers to the motion induced by the continuous flow of wind over time, while local turbulence or shorter-term movements contribute to dispersion. Pollutants within the atmosphere are transported to lower altitudes through deposition mechanisms, which include precipitation, scavenging, and sedimentation. Ultimately, these processes effectively remove the contaminants from the Earth's surface (1). Atmospheric Transport and Dispersion (ATD) models offer air quality professionals valuable insights into pollutant emissions, both pre- and post-emergency events. In these modeling studies, location, oscillation strength, and meteorological data assume crucial roles as inputs. Generally, meteorological data is readily accessible; however, determining the strength, location, and timing of emissions is a more challenging task (2). Notably, the presence of aerosol particles in the atmosphere necessitates attention to their potential impact on human health (3). The HYSPLIT model stands as the most widely utilized air trajectory model in the realm of research tools, owing to its capacity to trace the source-receptor relationship across considerable distances. This model calculates fundamental air parcel trajectories, facilitating the detection of extensive dispersion and deposition processes (4).

Environmental degradation and its detrimental consequences on human and animal health are predominantly attributable to air pollutants present in the atmosphere. Among these pollutants, particulate matter (PM), ozone (O_3), nitrogen dioxide (NO_2), volatile organic compounds (VOCs) - including those stemming from gasoline emissions - carbon

monoxide (CO), and sulfur dioxide (SO_2) have notable adverse effects on human well-being. Moreover, pollutants can be categorized as primary and secondary pollutants. Primary pollutants originate from various industrial activities, including those from industrial facilities and vehicles. In contrast, secondary pollutants are generated when primary pollutants undergo chemical reactions in the atmosphere (6).

1.1. HEALTH EFFECT OF AIR POLLUTION

Air pollutants exert detrimental effects not only on human and animal health but also on the overall environment. Any substance in the air that has an adverse impact on human well-being and environmental health is categorized as an air pollutant (5). Air pollution is widely recognized for its significant implications for human health. Among the numerous air pollutants, particulate matter (PM), ozone (O_3), nitrogen dioxide (NO_2), volatile organic compounds (VOCs), including those stemming from gasoline emissions, carbon monoxide (CO), and sulfur dioxide (SO_2) are notable contributors with significant health implications. Primary pollutants, such as gases emitted from motor vehicle exhausts, industrial sources, and those released during electricity and heat production, encompass substances like nitrogen and sulfur oxides. Secondary pollutants are generated as a result of chemical reactions involving primary pollutants and typically include ozone and particulate matter (6).

Particle Pollutants: Particulate pollutants constitute a significant portion of airborne pollutants and are typically a mixture of airborne particles (5). Particulate matter (PM) is categorized based on its size into coarse particles (diameter < 10 μm; PM_{10}), fine particles (diameter < 2.5 μm; $PM_{2.5}$), or very fine particles (<0.1 μm; $PM_{0.1}$). Generally, 50 % of the

total mass of PM_{10} is composed of $PM_{2.5}$, the fine particle fraction. PM_{10} primarily includes dust resuspension caused by wind and emissions from industrial and construction activities. On the other hand, $PM_{2.5}$ is primarily composed of emissions resulting from motor vehicle operations (both gasoline and diesel engines), electricity and heat generation, and industrial processes. $PM_{0.1}$, on the other hand, encompasses emissions from atmospheric photochemical reactions and vehicle exhaust (6). Fine and ultra-fine particles, in general, have adverse health effects as they can enter the body through the respiratory tract and the circulatory system. Exposure to particulate pollutants can lead to various health issues, including lung and heart diseases, as well as asthma, depending on the severity of the pollutants and the level of exposure (5).

Ground-Level Ozone: O_3 is a colorless gas typically found in the upper part of the atmosphere known as the troposphere. Ground-level ozone (GLO) forms as a result of human activities or the interaction of volatile organic compounds (VOCs) emitted from natural sources and chemical reactions with nitrogen oxides. Generally, GLO is associated with respiratory diseases (5).

Carbon Monoxide: CO is a colorless, odorless gas that is released into the atmosphere due to the combustion of fossil fuels (such as coal and wood) and can result in varying degrees of poisoning depending on the duration of exposure (5).

Sulfur Dioxide: SO_2 is a colorless and reactive gas that is released into the atmosphere due to the consumption of fossil fuels, industrial activities, or volcanic eruptions. SO_2 is generally a highly detrimental pollutant to living organisms and can lead to skin and lung diseases as a consequence of human exposure to this pollutant (5).

Nitrogen Oxide: NO is a significant pollutant emitted by motor vehicles and can result in respiratory tract infections (5).

Lead: Pb is a toxic heavy metal that can be introduced into the atmosphere, often stemming from industrial facilities. Pb accumulates in the bloodstream, bones, and various tissues within the body, adversely affecting the excretory system (including the kidneys and liver), nervous system, and other organs (5).

Other Air Pollutants: Additional air pollutants encompass Volatile Organic Compounds (VOCs), such as benzene, toluene, ethylbenzene, and xylene, which are released from industrial facilities, as well as Polycyclic Aromatic Hydrocarbons (PAHs), including acenaphthene, acenaphthylene, anthracene, and benzo[a]pyrene. These pollutants pose significant health risks to humans (5). The Environmental Protection Agency (EPA) standards for major air pollutants and their sources are detailed in Table 1.1.

Table 1.1 Standard level of criteria air pollutants and their sources with health impact based on the United States Environmental Protection Agency (5).

Air Pollutants	**Primary contributors of emissions**	**Averaging time**	**Standard concentration**	**Organs most affected by health effects**
$PM_{2.5}$	industrial processes, vehicle exhaust, and combustion of fossil fuels.	24 hours	35 $\mu g/m^3$	respiratory and cardiovascular diseases
PM_{10}		24 hours	150 $\mu g/m^3$	
Ground-level ozone	vehicles and industrial processes	1 hour	0.12 mg/m^3	respiratory and cardiovascular diseases
Carbon monoxide	vehicle exhaust, industrial processes, and residential heating using solid fuels like wood or coal	1 hour	35 mg/m^3	cardiovascular and central nervous system diseases
Sulfur dioxide	industrial processes, combustion of fossil fuels	1 hour	75 $\mu g/m^3$	respiratory and central nervous system diseases
Nitrogen dioxide	vehicles and industrial processes	1 hour	100 $\mu g/m^3$	respiratory and central nervous system diseases
Lead	industrial and manufacturing processes	3 months average	0.15 $\mu g/m^3$	central nervous system and respiratory diseases, hematologic disease
Polycyclic Aromatic Hydrocarbons (PAHs)	combustion of fossil fuel, wood	1 year	1 ng/m^3	cancer, respiratory and central nervous system diseases

1.1. DETECTION OF THE EFFECT OF AIR POLLUTANTS

The impact of air pollutants on health is typically contingent upon the concentration of the pollutant and the duration of exposure (7).

Pollutant Standard Index (PSI): PSI is a numerical value ranging from 0 to 500, which is utilized for risk assessment. The PSI value is determined by the concentrations of the five primary air pollutants: particulate matter (PM), sulfur dioxide (SO_2), nitrogen dioxide (NO_2), carbon monoxide (CO), and ground-level ozone (O_3) present in the air.

The Air Quality Index (AQI): AQI is a measure of air quality based on the requirements of various living species, including humans (5). The AQI is typically determined based on the concentrations of key pollutants, such as O_3, PM, CO, and SO_2 (7). The EPA's recommended AQI values are shown in Table 1.2.

Table 1.2 EPA recommended AQI value actions to protect health from particle pollution (8).

AQI colors	AQI value	Actions to protect one's health from particle pollution
	Good [0 - 50]	None
	Moderate [51 - 100]	People with chronic medical conditions should avoid strenuous activities and limit time spent outdoors.
	Unhealthy for sensitive groups [101 - 150]	People with heart or lung disease, children, and older adults should avoid prolonged outdoor exposure and strenuous exercise.
	Unhealthy [151 - 200]	People with heart or lung disease, children, and older adults should avoid outdoor exercise. Furthermore, it is recommended that all people avoid strenuous outdoor exercise.
	Very unhealthy [201 - 300]	People with heart or lung disease, children, and older adults should not go outside, and everyone should avoid outdoor physical activity.
	Hazardous [301 and higher]	Everyone is likely to be affected.

The AQI is divided into multiple health levels, ranging from 0 to over 300, each associated with a different level of health risk. It uses various color codes to convey air

quality and associated health concerns. Generally, green signifies healthy air quality, while yellow, orange, red, purple, and maroon indicate air quality that is unhealthy, very unhealthy, or hazardous for moderate and sensitive groups. These color codes may vary from one country to another (5).

1.2. ATMOSPHERIC DISPERSION MODELING

Modeling is a process that involves simulating and creating potential scenarios that may arise after a particular event. In the context of air quality, air pollutants are typically emitted into the atmosphere from various sources. These pollutant sources can be categorized as point sources, such as chimneys or vents, area sources, including dumps, ponds, and landfills, and volume sources, like conveyors and highly ventilated structures. The dispersion of pollutants released from these sources in the atmosphere is influenced by numerous factors. Dispersion models serve the purpose of estimating the ground-level concentration of emitted radiative substances. This estimation is made by taking into account available data regarding the emissions and the atmospheric conditions (9). Table 1.3 provides a list of potential data inputs for a dispersion model.

Types of Dispersion Models: The dispersion models vary from simple box-type models to complex fluid dynamics models, and these models differ depending on the variety of the medium and the relevant concentration parameters (9). Some sort of dispersion models are:

Box models: The simplest type of modeling is the box model, which represents the air chamber as a box. Although this model is useful, it has a few limitations. It is used to

calculate the average pollutant concentrations across a sizable region and makes the assumption that the pollutant is uniform throughout the air chamber (9).

Table 1.3 Potential Data Inputs for a Dispersion Model (10).

Emission Properties	**Characteristics of the Source**	**Characteristics of the Location**	**Atmospheric Features**
Pollutants	Source types (e.g. point, line, area, volume)	Location (e.g. urban vs rural)	Temperature
Pollutant characteristics	Source dimensions (if applicable)	Landscape (simple vs complex)	Wind speed
Distribution of source(s)	Volume emission rates	Surface roughness	Wind direction
Emission rates	Temperature	Interfaces of ground & water (if any)	Atmospheric stability/turbulence
	Moisture content	Existing levels of pollutants in the background.	Solar radiation (especially critical in photochemical modeling)
	Presence of structure or other infrastructure		Cloud cover
			Moisture

Eulerian models: Eulerian models divide the study area into a series of grid cells, both horizontal and vertical to calculate the average pollutant concentration within each grid cell at the time point. The original purpose of the Eulerian models was to simulate time periods that lasted for only a few days per simulation. However, modern versions of these models can be used to simulate longer time periods. The benefit of Eulerian models is that they are able to account for the removal of constituent particles through deposition or chemical reactions as they are based on average grid concentrations rather than tracking an entire plume (10).

Gaussian models: It is the most used model in air distribution models. A mathematical model known as the Gaussian model is predicated on the notion that a

pollutant would spread in accordance with its typical statistical distribution (9). Gaussian models assume that plume dispersion is mainly due to the diffusion of constituent pollutants, and that the concentration of pollutants follows a normal distribution both horizontally and vertically. Gaussian models generally assume that pollutants move at a constant speed and are modeled accordingly. Furthermore, Gaussian plumes always expand in the y and z directions. Gaussian dispersion models assume that emission and meteorological conditions are constant, chemical reactions are not required, and wind speeds are always 1 m/s or more (10).

The Gaussian model takes into account various factors such as pollutant release rate and height, wind speed, mixing/inversion height, and horizontal and vertical dispersion factors as inputs to accurately predict the spread and concentration of pollutants in the atmosphere. In addition, the plume's upward or downward movement can be simulated. Another important aspect of Eulerian models is that when smoke or pollutants reach the ground or the upper boundary layer of air, it is assumed that they are quantitatively reflected from these surfaces. This can create a false image of pollutants accumulating at ground level over time. However, this effect can also be accounted for in the model, thus providing a more accurate representation of the pollution levels (10).

- **Atmospheric Stability**

The shapes of plumes rely on the levels of atmospheric stability, which depend on the Dry Adiabatic Lapse Rate (DALR) and Environmental Lapse Rate (ELR). The Atmospheric Lapse Rate (ALR) plays a crucial role in determining the vertical stability of air and the formation of clouds with significant vertical development. DALR is a term used to describe the way temperature changes in the atmosphere as altitude increases or

decreases. It is a ratio that expresses the temperature change of a mass of air as it rises or falls. ELR refers to the actual vertical distribution of air temperature in the atmosphere. This distribution can sometimes be unstable, which may trigger the formation of thermals, especially if other triggering mechanisms are also present (11).The following are the stability conditions based on ELR and DALR (9):

- ✓ ELR > DALR, atmosphere is stable,
- ✓ ELR >>DALR, very stable atmosphere,
- ✓ ELR = DALR, atmosphere is neutral,
- ✓ ELR <DALR, atmosphere is unstable.

Lagrangian model: When predicting the dispersion of pollutants, a moving reference grid is often used. This grid is typically based on the prevailing wind direction or the overall movement of the dust plume. Unlike models, which estimate pollutant concentration using a moving reference grid, measurements are often taken at fixed sites (9). Lagrangian models work by simulating a series of pollutant "puffs", which are emitted from the source at regular intervals. It is commonly known as the Gaussian puff model and assumes that each puff moves in the direction of the wind and expands following the Gaussian distribution at the same time. A model consists of hundreds or thousands of theoretical puffs, which are 3D elements that can expand in all dimensions and move downwards. Overall, when examining each puff separately, variations in dispersion rates and directions become apparent. This allows for a more realistic modeling of local conditions in the simulation. Another version of the Lagrangian model is the Lagrangian random walk model. In this model, the puff is broken down into several independent tracer

particles. These particles are then transported by the mean wind field with local turbulence using a stochastic random walk algorithm (10).

Lagrangian models have been proven to offer higher accuracy in models that involve complex topography or flow patterns, such as the recirculation of pollutants, and in cases where there is temporal variation in emissions or meteorology. Lagrangian models are frequently employed for modeling over longer distances and timeframes, with some models capable of spanning several years. In contrast, Gaussian plume models are usually limited to forecasts within 50 km of the point source. Time steps ranging from 1 to 180 seconds are often used in Lagrangian models. Just like in Gaussian plume modeling, the assumption of total pollutant reflection from the ground and upper atmospheric boundary layer in Lagrangian models may lead to incorrect conclusions if not appropriately accounted for (10).

1.3. HYSPLIT MODELING PROGRAM

The Hybrid Single Particle Lagrangian Integrated Orbital model (HYSPLIT), developed by the National Oceanic and Atmospheric Administration (NOAA) Air Resources Laboratory (ARL), is a versatile tool for simulating a wide range of atmospheric processes, including atmospheric oscillation, transport, chemical deposition, and transformation (9). Similar to the HYSPLIT model, it allows for the calculation of the distribution, accumulation, and location of regional assumptions simultaneously (13).

Atmospheric dispersion models are generally categorized into two types: Eulerian and Lagrangian. The HYSPLIT model falls into the Lagrangian category, meaning it primarily relies on meteorological fields related to the calculation point when determining

pollutant distribution (14). In the Lagrangian approach, meteorological factors play a significant role, and it tracks how pollutants change from their initial positions. In contrast, the Eulerian approach heavily relies on grid-based modeling and considers changes in pollutant concentrations (15).

The HYSPLIT model is applied in various simulation studies, including monitoring pollutant releases, tracking air parcel trajectories, studying smoke plumes resulting from forest fires and volcanic ash, and forecasting based on its capabilities. Grid meteorological data is essential for both backward and forward trajectory analysis and concentration calculations using the HYSPLIT model. This data provides information on vertical spreading profiles, wind shear, and wind fields' horizontal deformation (16). Additionally, air concentrations are typically calculated by averaging concentrations at specific grid points within a cell. For forecasting purposes, observational data is incorporated using the Global Forecast System (GFS), and meteorological data output is generated based on the grid model area using the Global Data Assimilation System (GDAS) within HYSPLIT (17).

When calculating pollutant distribution in HYSPLIT, the model offers two modes: 3-D particle mode or puff mode. These modes allow for calculations based on the required grid meteorological data, and they are chosen based on the specific requirements of the study (18).

In the puff model, the pollutant initially expands both horizontally and vertically to match the dimensions of the meteorological grid cell, and then it undergoes a process of contraction. During this contraction phase, it is divided into new puffs, with each new puff containing a fraction of the original pollutant mass. A predetermined number of initial

particles are distributed across the entire model domain, utilizing both the mean wind field and a turbulent component incorporated into the particle model (19).

HYSPLIT typically employs meteorological input data from various sources, including other meteorological models and archived gridded meteorological data fields. Users have the flexibility to define the extent of wind data they wish to utilize within the system. HYSPLIT employs interpolation techniques to adapt the meteorological data at each horizontal grid point from the meteorological input data to an internal sub-grid. This sub-grid employs a terrain-following coordinate system where all heights are referenced relative to mean sea level. It's worth noting that different meteorological models may use varying vertical coordinate systems, highlighting the importance of this interpolation process (13).

Backward trajectories are used to estimate the approximate 3D transport of an air parcel by relying on archived wind field and pressure data. These trajectories are instrumental in identifying the geographical source regions of various atmospheric components and conducting backward trajectory analysis. The accuracy of this trajectory analysis is contingent on factors such as the resolution of the wind field data, the relevant meteorological data, and the calculation methods applied (20).

Cluster techniques are commonly employed to determine the primary transit routes of air mass backward trajectories. There are three distinct approaches for time series analysis: the raw-data-based approach, the feature-based approach, and the model-based approach. Trajectory clustering is a specific issue in time series analysis (21).

To generate trajectories using the HYSPLIT modeling program, location information such as latitude, longitude, and the initial height above ground level (AGL) is

provided. In this research, an AGL initial height of 500 meters was selected. For the cluster analysis, four new trajectory calculations were performed, with a new trajectory generated every 6 hours over the course of a day. Trajectory Cluster Analysis is typically based on latitude and longitude, with altitude and external factors not factored into the analysis. The number of trajectories to be calculated during a clustering hour is determined, and the time interval dictates the endpoints used. In this research, 240 hours were calculated separately for each month as the clustering hours, and a 6-hour time interval was employed. The total spatial variance (TSV) for this analysis was found to be zero (22).

In the analysis, there were N trajectories, and each trajectory was regarded as a distinct cluster. The cluster spatial variance (SPVAR) was determined as the sum of the squared distances between the endpoints of the component trajectories within a cluster and the mean trajectory of that cluster. To obtain the total spatial variance (TSV), the sum of all cluster spatial variances was computed. The identification of the number of clusters was achieved through cluster analysis, which involved observing sudden drops in TSV (22).

Figure 1.1 illustrates the change in Total Spatial Variance (TSV) for January 2021 in the backward trajectory calculation. Based on the TSV, the analysis determined the presence of three clusters, and 125 backward trajectories were identified. Figure 1.2 provides further details on the number of backward trajectories in January 2021. In contrast, Figure 1.3 displays the Total Spatial Variance (TSV) changes during the forward trajectory calculation for January, which also resulted in three clusters and 125 forward trajectories. The number of forward trajectories in January 2021 is depicted in Figure 1.4.

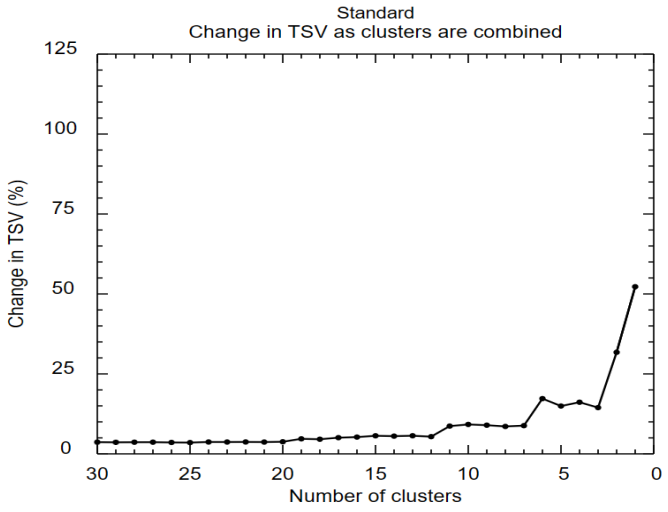

Figure 1.1 A graph showing the change in Total Spatial Variance (TSV) for January 2021 in the backward trajectory calculation.

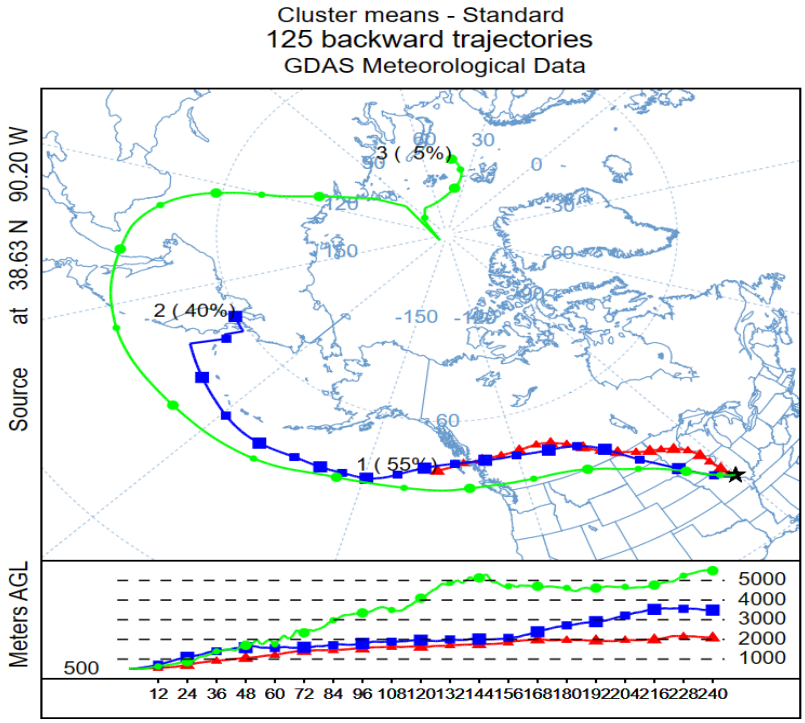

Figure 1.2 The number of backward trajectories in St. Louis in January 2021.

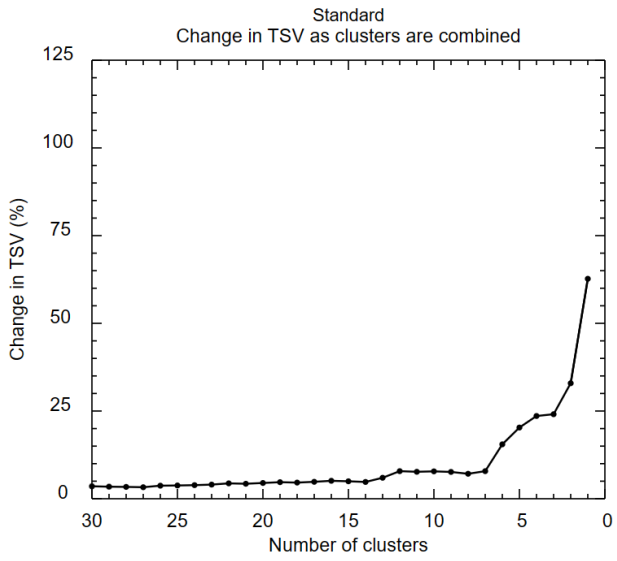

Figure 1.3 A graph showing the change in Total Spatial Variance (TSV) for January in the forward trajectory calculation.

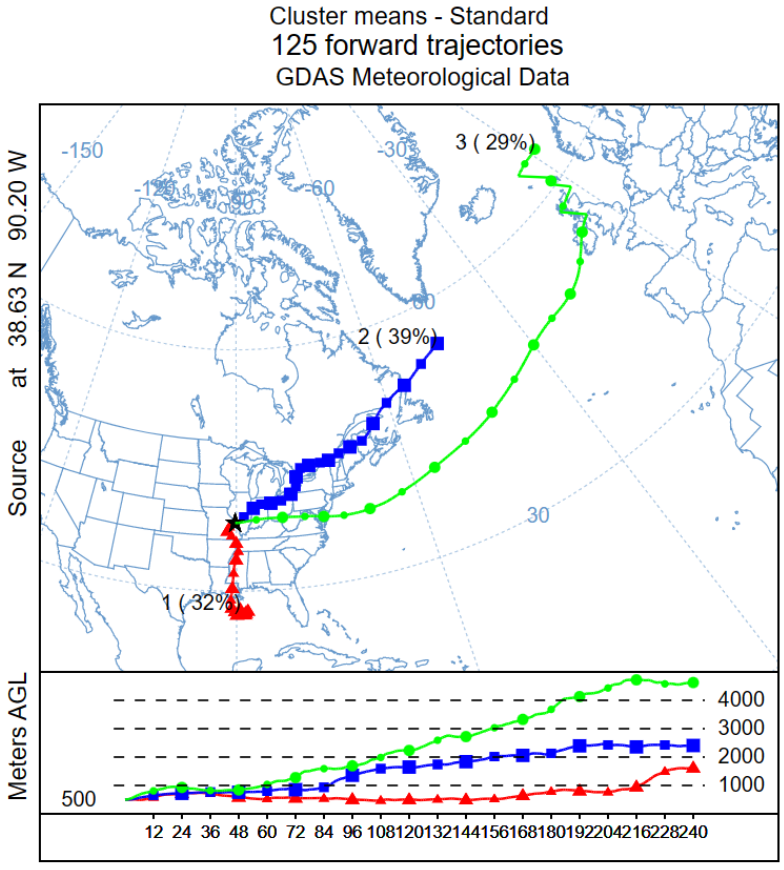

Figure 1.4 The number of forward trajectories in St. Louis in January 2021.

1.4. RESEARCH OBJECTIVES

This research aimed to determine the atmospheric transport and dispersion of any hazardous aerosols in St. Louis. This study's objectives were:

- Generate monthly and seasonal backward trajectory and cluster analysis of air mass in St. Louis for the years 2020, 2021, and 2022.
- Analyze air pollution data in St. Louis for the years 2020, 2021, and 2022.
- Utilize the HYSPLIT modeling program to gain insights into the sources and atmospheric dispersion of pollution in St. Louis during the years 2020, 2021, and 2022.

2. MONTHLY AND SEASONAL BACKWARD TRAJECTORY ANALYSIS OF AIR MASS IN ST. LOUIS

The coordinates of St. Louis are 38.627 latitude and -90.199 longitude. Subsequently, back trajectory analysis was conducted based on these coordinates, with an altitude of 500 meters.

2.1. MONTHLY BACKWARD TRAJECTORY ANALYSIS OF AIR MASS IN ST. LOUIS

Backward trajectory and cluster analyses were generated for the periods of January 2020 to December 2020, January 2021 to December 2021, and January 2022 to December 2022 using the HYSPLIT modeling program. Prior to calculating the backward trajectory and cluster analysis, the Global Data Assimilation System (GDAS) data for each respective month was downloaded. Calculations were performed over a total of 240 hours backward in 6-hour intervals.

2.1.1. Backward Trajectory Analysis of Air Masses from January 2020 to December 2020 in St. Louis. Backward trajectory and cluster analyses were conducted using the HYSPLIT modeling program for the period from January 2020 to December 2020. These calculations involved a total of 240 hours backward in 6-hour time intervals.

Figure 2.1 (a) depicts the number of backward trajectories in January 2020. According to the Total Spatial Variance (TSV), there were three clusters, and a total of 125 backward trajectories were identified for January 2020. The number of backward trajectories for January 2020 revealed three clusters, including one trajectory followed by 55 % of clusters that originated near Canada in the Pacific Ocean, passed through the

western United States, and ended up in St. Louis from the northwestern United States. Another trajectory, followed by 29 % of clusters, began in the Pacific Ocean, passed through the western United States, and arrived in St. Louis. The last trajectory, followed by 16 % of clusters, started in an area in the Arctic Ocean, moved over Russia, and found a route through the Bering Sea, the Pacific Ocean, and Canada before reaching St. Louis from the northern United States.

Figure 2.1 (b) illustrates the number of backward trajectories in February 2020. According to TSV, there were three clusters, and a total of 117 backward trajectories were identified for February 2020. In February 2020, there were three clusters, including one trajectory followed by 49 % of clusters that commenced near Canada in the Pacific Ocean, passed through the western United States, and ended up in St. Louis from the northwestern United States. Another trajectory, followed by 29 % of clusters, initiated near Russia in the Sea of Okhotsk, traversed through the Pacific Ocean via a route through Canada, and reached St. Louis from the northwest United States. The last trajectory, followed by 22 % of clusters, began in an area in the Arctic Ocean, proceeded through Canada, and arrived in St. Louis from the northern United States.

Figure 2.1 (c) displays the number of backward trajectories in March 2020. According to TSV, there were three clusters, and a total of 125 backward trajectories were identified for March 2020. The backward trajectories for March 2020 revealed three clusters, including one trajectory followed by 26 % of clusters that originated from a region in Russia. It proceeded northwest through the Sea of Okhotsk, crossed over the Bering Sea, found a route through Canada, and ended in St. Louis from the northern United States. Another trajectory, followed by 64 % of clusters, started near Canada in the Pacific Ocean,

passed through the western United States, and arrived in St. Louis from the northwestern United States. The last trajectory, followed by 10 % of clusters, commenced in the Pacific Ocean, moved over the Gulf of Mexico, and reached St. Louis from the southern United States. Table 2.1 presents information, including the number of trajectories, cluster percentages, starting points, and directions for January, February, and March 2020.

Table 2.1 The number of trajectories, percentage of clusters, starting points and directions for January, February, and March 2020.

Month	Number of trajectories	Percentile of clusters	Starting location	Directions
January 2020	3	55 %	near Canada in The Pacific Ocean	the western directions
		29 %	The Pacific Ocean	the northwestern direction
		16 %	The Arctic Ocean	the northern direction
February 2020	3	49 %	near Canada in The Pacific Ocean	the western direction
		29 %	The sea of Okhotsk	the northwestern direction
		22 %	The Arctic Ocean	the northern direction
March 2020	3	26 %	Russia	the northern direction
		64 %	near Canada in The Pacific Ocean	the northwestern direction
		10 %	The Pacific Ocean	the southern direction

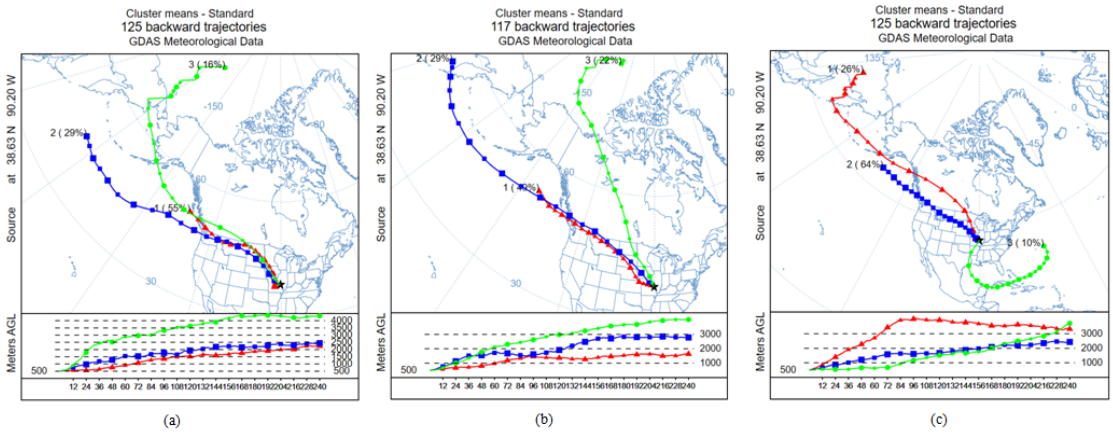

Figure 2.1 The number of backward trajectories (a) January 2020, (b) February 2020, (c) March 2020.

Figure 2.2 (a) illustrates the number of backward trajectories in April 2020. According to TSV, there were three clusters, and a total of 121 backward trajectories were identified for April 2020. The backward trajectories for April 2020 revealed three clusters, including one trajectory followed by 34 % of clusters that originated near Russia in the Pacific Ocean. It moved through the Gulf of Alaska, passed through Canada, and reached St. Louis from the northern United States. Another trajectory, followed by 59 % of clusters, began somewhere in Canada and traveled to St. Louis. The last trajectory, followed by 7 % of clusters, commenced in the Arctic Ocean, proceeded through the North Pole using a route through Canada, and ended in St. Louis from the northern United States.

Figure 2.2 (b) illustrates the number of backward trajectories in May 2020. According to TSV, there were four clusters, and a total of 124 backward trajectories were identified for May 2020. The backward trajectories for May 2020 revealed four clusters. One of these trajectories, followed by 31 % of clusters, initiated somewhere in the Pacific Ocean, moved through the western United States, and ended in St. Louis. Another trajectory, followed by 31 % of clusters, began on King William Island in Canada and traveled to St. Louis from the northern United States. An additional trajectory, followed by 8 % of clusters, commenced near China in the Yellow Sea, passed through the Pacific Ocean, traveled through Canada, and arrived in St. Louis from the northwestern United States. The last trajectory, followed by 29 % of clusters, started somewhere near Virginia in the Pacific Ocean. It moved southward and northward, passed through North Carolina, and found a pathway through Georgia, Alabama, and Tennessee before reaching St. Louis. Table 2.2 presents information, including the number of trajectory, cluster percentages, starting points, and directions for April, May, and June 2020.

Table 2.2 The number of trajectories, percentage of clusters, starting points and directions for April, May, and June 2020.

Month	Number of trajectories	Percentile of clusters	Starting location	Directions
April 2020	3	34 %	near Russia in The Pacific Ocean	the northern direction
		59 %	Canada	the northwestern direction
		7 %	The Arctic Ocean	the northern direction
May 2020	4	31 %	The Pacific Ocean	the northern direction
		31 %	King William Island in Canada	the northern direction
		8 %	near China in Yellow Sea	the northwestern direction
		29 %	near Virginia in The Pacific Ocean	the southeastern direction
June 2020	3	46 %	Canada	the northern direction
		19 %	Kuril Islands	the western direction
		35 %	The Atlantic Ocean	the southern direction

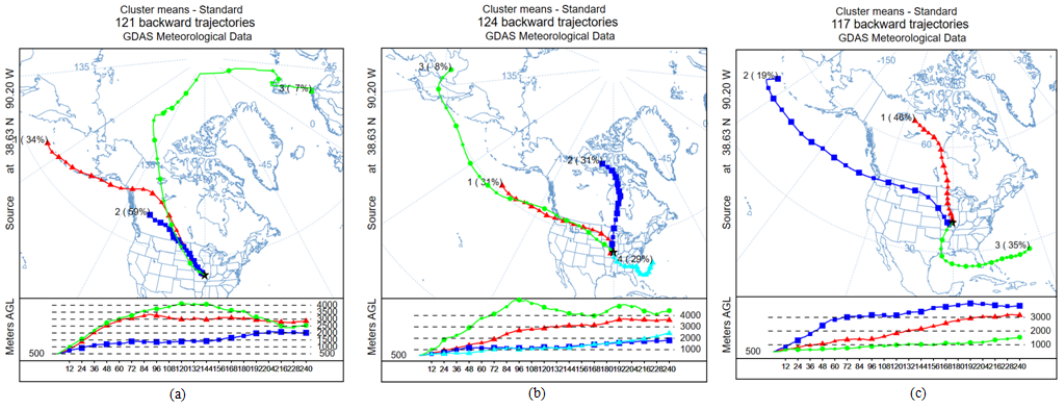

Figure 2.2 The number of backward trajectories (a) April 2020, (b) May 2020, (c) June 2020.

Figure 2.2 (c) illustrates the number of backward trajectories in June 2020. According to TSV, there were three clusters, and a total of 117 backward trajectories were identified for June 2020. The backward trajectories for June 2020 revealed three clusters, including one trajectory followed by 46 % of clusters. It began in the northern region of Canada and ended in St. Louis from the northern United States. Another trajectory, followed by 19 % of clusters, started from the Kuril Islands, moved through the Pacific

Ocean, passed through the western United States, and arrived in St. Louis. The last trajectory, followed by 35 % of clusters, originated from the Atlantic Ocean, moved through Florida, traveled through the Gulf of Mexico, and ended in St. Louis from the southern United States.

Figure 2.3 (a) illustrates the number of backward trajectories in July 2020. According to TSV, there were two clusters, and a total of 124 backward trajectories were identified for July 2020. In July 2020, there were two clusters. One of these trajectories, followed by 69 % of clusters, originated somewhere in the Atlantic Ocean. It moved through Georgia, Alabama, Mississippi, using a pathway through Arkansas, and arrived in St. Louis from the southern United States. The last trajectory, followed by 31 % of clusters, started somewhere in the Pacific Ocean, moved through Canada, and reached St. Louis from the northwestern United States. Table 2.3 presents information, including the number of trajectories, cluster percentages, starting points, and directions for July, August, September 2020.

Table 2.3 The number of trajectories, percentage of clusters, starting points and directions for July, August, September 2020.

Month	Number of trajectories	Percentile of clusters	Starting location	Directions
July 2020	2	69 %	The Atlantic Ocean	the southern direction
		31 %	The Pacific Ocean	the northwestern direction
August 2020	5	30 %	the west of Gulf of Hudson in Canada	the northern direction
		27 %	The Pacific Ocean	the northwestern direction
		11 %	the north of Alaska	the northern direction
		19 %	the west of Colorado	the western direction
		12 %	The Atlantic Ocean	the southern direction
September 2020	4	36 %	Canada	the northwestern direction
		20 %	Kentucky	the northern direction
		26 %	Kuril Islands	the western direction
		18 %	The Arctic Ocean	the northern direction

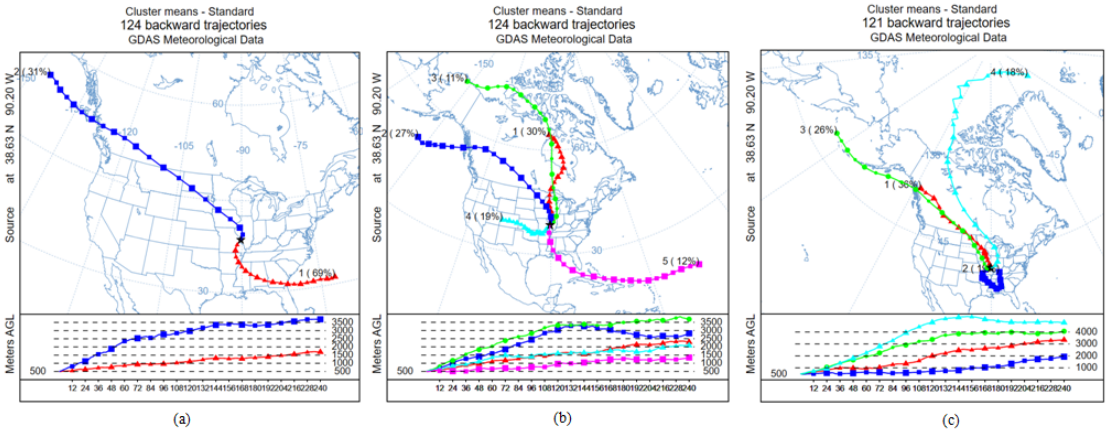

Figure 2.3 The number of backward trajectories (a) July 2020, (b) August 2020, (c) September 2020.

Figure 2.3 (b) illustrates the number of backward trajectories in August 2020. According to TSV, there were five clusters, and a total of 124 backward trajectories were identified for August 2020. In August 2020, there were five clusters, including one trajectory followed by 30 % of clusters, which originated from the west of the Gulf of Hudson in Canada and ended in St. Louis from the northern United States. Another trajectory, followed by 27 % of clusters, started somewhere in the Pacific Ocean, passed through Canada, and traversed to St. Louis from the northwestern United States. Another trajectory, followed by 11 % of clusters, commenced in the north of Alaska and moved through Queen Elizabeth Islands in Canada, reaching St. Louis from the northern United States. Additionally, a trajectory followed by 19% of clusters started from the west of Colorado, passed through Kansas and Oklahoma, and ended in St. Louis. Lastly, a trajectory followed by 12 % of clusters began in the Atlantic Ocean, moved through the Dominican Republic, Cuba, and the Gulf of Mexico, and arrived in St. Louis from the southern United States.

Figure 2.3 (c) depicts the number of backward trajectories in September 2020. According to TSV, there were four clusters, and a total of 121 backward trajectories were identified for September 2020. The backward trajectories for September 2020 revealed four clusters. One of these trajectories, followed by 36 % of clusters, began somewhere in Canada and traversed to St. Louis from the northwestern United States. Another trajectory, followed by 20 % of clusters, started in Kentucky, moved through Tennessee to Alabama from the northern United States, and then turned through Mississippi and Arkansas before reaching St. Louis from the southern United States. An additional trajectory, followed by 26 % of clusters, initiated from the Kuril Islands, moved through the Pacific Ocean and Canada, and arrived in St. Louis from the western United States. The last trajectory, followed by 18 % of clusters, started somewhere in the Arctic Ocean, proceeded through Canada, and reached St. Louis from the northern United States.

Figure 2.4 (a) illustrates the number of backward trajectories in October 2020. According to TSV, there were three clusters, and a total of 125 backward trajectories were identified for October 2020. In October 2020, there were three clusters, one of which was a trajectory followed by 30 % of clusters. It originated in Russia, moved through the Sea of Okhotsk, traveled through the Pacific Ocean via a route through Canada, and ended in St. Louis from the northwest United States. Another trajectory, followed by 61 % of clusters, started in Alaska, moved through Canada, and reached St. Louis from the northwestern United States. The last trajectory, followed by 10 % of clusters, began in the Atlantic Ocean, moved through Florida, Alabama, Mississippi, and Arkansas, and traveled to St. Louis from the southern United States. Table 2.4 presents information, including the

number of trajectories, cluster percentages, starting points, and directions for October, November, and December 2020.

Table 2.4 The number of trajectories, percentage of clusters, starting points and directions for October, November, and December 2020.

Month	Number of trajectories	Percentile of clusters	Starting location	Directions
October 2020	3	30 %	Russia	the northwestern direction
		61 %	Alaska	the northwestern direction
		10 %	The Atlantic Ocean	the southern direction
November 2020	2	77 %	The sea of Okhotsk	the northwestern direction
		23 %	East Siberian Sea	the northwestern direction
December 2020	3	50 %	The Gulf of Alaska	the northwestern direction
		44 %	Russia	the western direction
		6 %	Russia	the northwestern direction

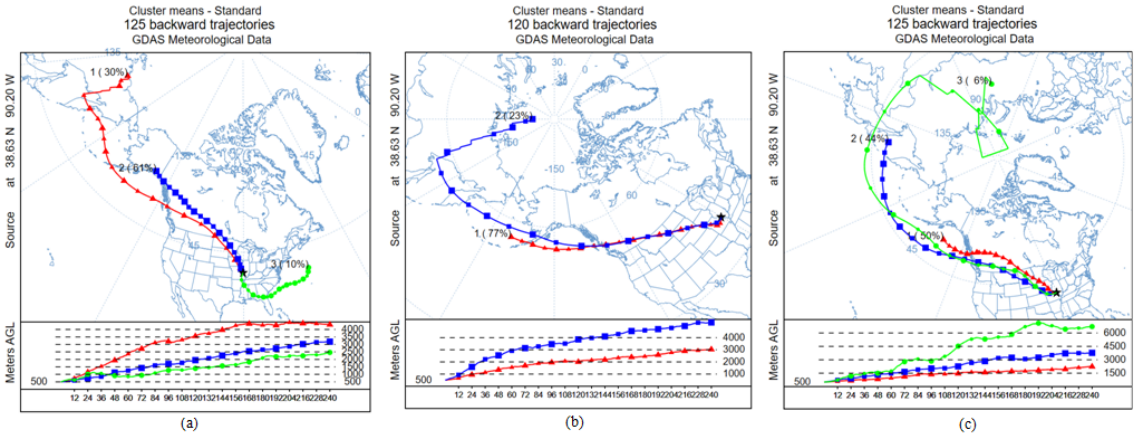

Figure 2.4 The number of backward trajectories (a) October 2020, (b) November 2020, (c) December 2020.

Figure 2.4 (b) illustrates the number of backward trajectories in November 2020. According to TSV, there were two clusters, and a total of 120 backward trajectories were identified for November 2020. In November 2020, there were two clusters, one of which was a trajectory followed by 77 % of clusters. It commenced from the Sea of Okhotsk, moved through the Pacific Ocean, and found a pathway through Canada, eventually

arriving in St. Louis from the northwestern United States. The last trajectory, followed by 23 % of clusters, began somewhere in the East Siberian Sea, moved through Russia, and took a route through the Sea of Okhotsk, Bering Sea, the Gulf of Alaska, and Canada, finally reaching St. Louis from the northwestern United States.

Figure 2.4 (c) illustrates the number of backward trajectories in December 2020. According to TSV, there were three clusters, and a total of 125 backward trajectories were identified for December 2020. In December 2020, there were three clusters, one of which was a trajectory followed by 50 % of clusters. It started from somewhere in the Gulf of Alaska, moved through Canada, and ended in St. Louis from the northwest United States. Another trajectory, followed by 44 % of clusters, began near Russia in the Sea of Okhotsk, moved over through the Pacific Ocean and Canada, and traversed to St. Louis from the western United States. The last trajectory, followed by 6 % of clusters, originated in Russia, traveled northward, then returned from the North Pole, moved through Mongolia, China, and the Pacific Ocean via a pathway through Canada, and arrived in St. Louis from the northwestern United States.

2.1.2. Backward Trajectory Analysis of Air Masses from January 2021 to December 2021 in St. Louis. Backward trajectory and cluster analysis were generated from January 2021 to December 2021 on the HYSPLIT modeling program. The calculation was made according to 240 total hours backward and 6-hour time intervals.

Figure 2.5 (a) shows the number of backward trajectories in January 2021. According to TSV, the number of clusters was three, and 125 backward trajectories were found for January 2021. There were three clusters in January 2021, one of which was a trajectory followed by 55 % of clusters starting from an area in the Pacific Ocean and

traveled through Canada and traversed to St. Louis from the northwest United States, another trajectory followed by 40 % of clusters started from a region in Russia and moved through the Pacific Ocean and found a pathway through Canada to St. Louis from the northwest United States, and the last trajectory followed by 5 % of clusters started near the North Pole and found a route through Russia and the Pacific Ocean and traversed to St. Louis from the northwestern United States. Table 2.5 shows information including the number of trajectories, cluster percentage, starting points and directions for January, February, and March 2021.

Table 2.5 The number of trajectories, percentage of clusters, starting points and directions for January, February, and March 2021.

Month	Number of trajectory	Percentile of clusters	Starting location	Directions
January 2021	3	55 %	The Pacific Ocean	the northwestern direction
		40 %	Russia	the northwestern direction
		5 %	near The North Pole	the northwestern direction
February 2021	3	56 %	Canada	the northern direction
		22 %	Russia	the northwestern direction
		22 %	Idaho	the northwestern direction
March 2021	4	42 %	The Pacific Ocean	the northwestern direction
		31 %	Russia	the northwestern direction
		21 %	Canada	the northeastern direction
		6 %	near The North Pole	the northern direction

Figure 2.5 (b) illustrates the number of backward trajectories in February 2021. According to TSV, there were three clusters, and a total of 113 backward trajectories were identified for February 2021. In February 2021, there were three clusters, one of which was a trajectory followed by 56 % of clusters. It started from a region in Canada and traveled to St. Louis from the north. Another trajectory, followed by 22 % of clusters, began in a region in Russia, headed northwest through the Pacific Ocean, moved over through

Canada, and traversed to St. Louis from the northwestern United States. The last trajectory, followed by 22 % of clusters, started from Idaho and traveled to St. Louis.

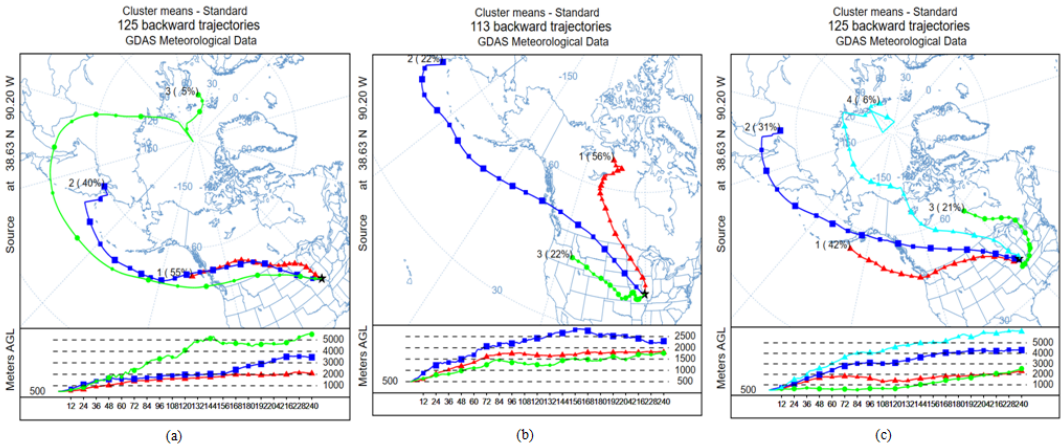

Figure 2.5 The number of backward trajectories (a) January 2021, (b) February 2021, (c) March 2021.

Figure 2.5 (c) illustrates the number of backward trajectories in March 2021. According to TSV, there were four clusters, and a total of 125 backward trajectories were identified for March 2021. In March 2021, there were four clusters, one of which was a trajectory followed by 42 % of clusters, starting from near Alaska in the Pacific Ocean, and traveling through the western United States to reach St. Louis from the northwestern United States. Another trajectory, followed by 31 % of clusters, started from Russia, traversed through the Pacific Ocean, and moved through Canada to reach St. Louis. Another trajectory, followed by 21 % of clusters, started from Canada and traveled to St. Louis from the northeastern United States. The last trajectory, followed by 6% of clusters, began near the North Pole, took a route through the Arctic Ocean, moved through Canada, and traversed to St. Louis from the northern United States.

Figure 2.6 (a) illustrates the number of backward trajectories in April 2021. According to TSV, there were four clusters, and a total of 121 backward trajectories were identified for April 2021. In April 2021, there were four clusters, one of which was a trajectory followed by 20 % of clusters, starting from the Pacific Ocean and moving through the northwest to reach St. Louis from the southwestern United States. Another trajectory, followed by 28 % of clusters, started from Russia and traveled through Alaska, using a pathway through Canada, and arrived in St. Louis. Another trajectory, followed by 49 % of clusters, began in Canada and reached St. Louis. The last trajectory, followed by 3 % of clusters, started from the Atlantic Ocean, moved over the Caribbean Sea, using a pathway through the Gulf of Mexico, and traversed to St. Louis from the southern United States.

Figure 2.6 (b) illustrates the number of backward trajectories in May 2021. According to TSV, there were three clusters, and a total of 125 backward trajectories were identified for May 2021. In May 2021, there were three clusters, one of which was a trajectory followed by 22 % of clusters, starting from the Pacific Ocean and moving through the western United States to reach St. Louis. Another trajectory, followed by 33 % of clusters, began in Canada and traveled along the east coast of the United States, finding a pathway through the southern United States before reaching St. Louis. The last trajectory, followed by 46 % of clusters, originated near the Northwest Gateway in Canada and reached St. Louis from the northern United States. Table 2.6 provides information, including the number of trajectories, cluster percentages, starting points, and directions for the months of April, May, and June 2021.

Table 2.6 The number of trajectories, percentage of clusters, starting points and directions for April, May, and June 2021.

Month	Number of trajectories	Percentile of clusters	Starting location	Directions
April 2021	4	20 %	The Pacific Ocean	the northwestern direction
		28 %	Russia	the northwestern direction
		49 %	Canada	the northwestern direction
		3 %	The Atlantic Ocean	the southern direction
May 2021	3	22 %	The Pacific Ocean	the western direction
		33 %	Canada	the southern direction
		46 %	The Northwest Gateway in Canada	the northern direction
June 2021	3	26 %	near Alaska in Bering Sea	the northwestern direction
		36 %	Canada	the northern direction
		38 %	The Atlantic Ocean	the southern direction

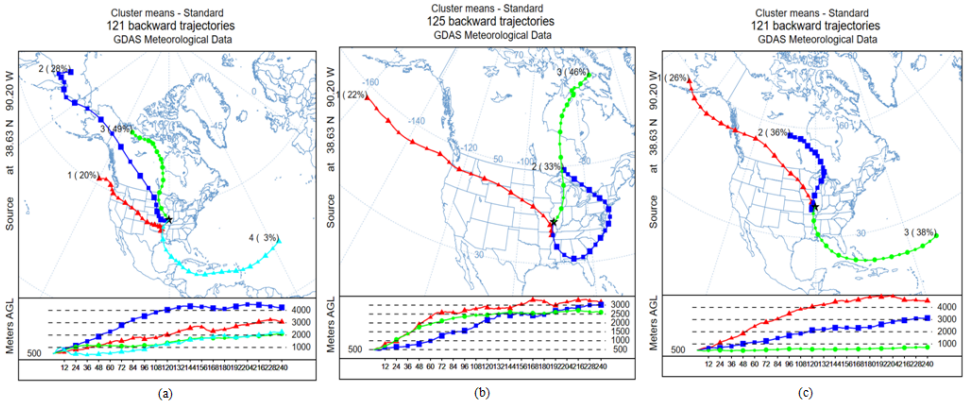

Figure 2.6 The number of backward trajectories (a) April 2021, (b) May 2021, (c) June 2021.

Figure 2.6 (c) illustrates the number of backward trajectories in June 2021. According to TSV, there were three clusters, and a total of 121 backward trajectories were identified for June 2021. Among these clusters, one trajectory was followed by 26 % of the clusters, starting near Alaska and traversing through Canada to reach St. Louis. Another trajectory, followed by 36 % of the clusters, began in Canada and ended in St. Louis. The last trajectory, followed by 38 % of the clusters, originated from the Atlantic Ocean, crossed the Gulf of Mexico, and finally arrived in St. Louis from South America.

Figure 2.7 (a) depicts the number of backward trajectories in July 2021. According to TSV, there were two clusters, and a total of 125 backward trajectories were identified for July 2021. Among these clusters, one trajectory, followed by 25 % of the clusters, originated from the Atlantic Ocean, passed through the Gulf of Mexico, and ended in St. Louis, coming from the southern United States. The other trajectory, followed by 75 % of the clusters, began in Canada and reached St. Louis.

Figure 2.7 (b) illustrates the number of backward trajectories in August 2021. According to TSV, two clusters were identified, with a total of 125 backward trajectories for August 2021. One trajectory, followed by 45 % of clusters, originated in Canada and ended in St. Louis, while the remaining trajectory, followed by 55 % of clusters, began in the Atlantic Ocean, passed through Florida, and proceeded through Louisiana and Arkansas before reaching St. Louis.

Figure 2.7 (c) illustrates the number of backward trajectories in September 2021. According to TSV, there were three clusters, and 121 backward trajectories were identified for September 2021. The trajectories revealed three clusters, one of which depicted a path followed by 18 % of clusters originating from the Atlantic Ocean, crossing Florida, and arriving in St. Louis from the southeastern United States. Another trajectory was traced by 42 % of clusters, commencing in Canada and ending in St. Louis from the northern United States. The remaining trajectory, representing 40 % of clusters, began somewhere in the Bering Sea, transited through Canada, and reached St. Louis. Table 2.7 provides information, including the number of trajectories, cluster percentages, starting points, and directions for July, August, and September 2021.

Table 2.7 The number of trajectories, percentage of clusters, starting points and directions for July, August, and September 2021.

Month	Number of trajectories	Percentile of clusters	Starting location	Directions
July 2021	2	25 %	The Atlantic Ocean	the southern direction
		75 %	Canada	the northern direction
August 2021	2	45 %	Canada	the northern direction
		55 %	The Atlantic Ocean	the southern direction
September 2021	3	18 %	The Atlantic Ocean	the southeastern direction
		42 %	Canada	the northern direction
		40 %	Bering Sea	the northwestern direction

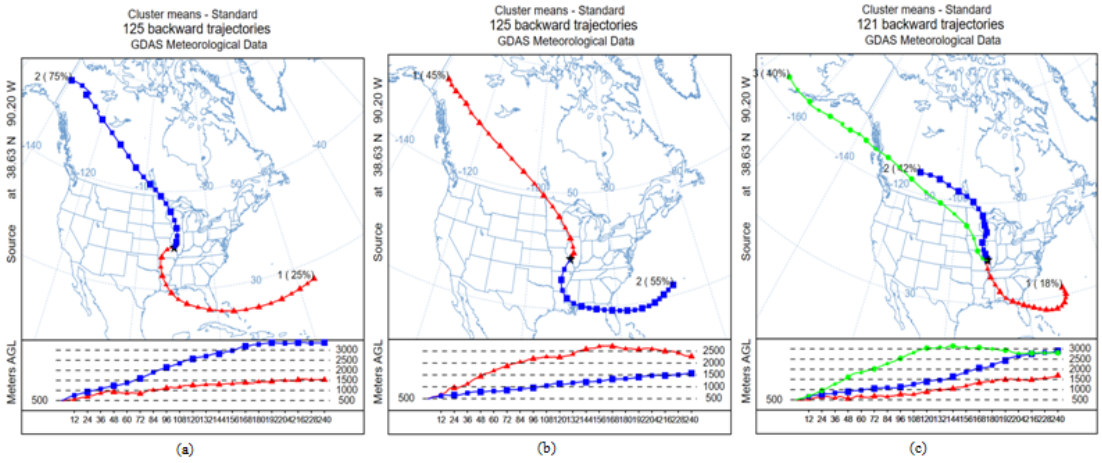

Figure 2.7 The number of backward trajectories (a) July 2021, (b) August 2021, (c) September 2021.

Figure 2.8 (a) illustrates the number of backward trajectories in October 2021. According to TSV, there were three clusters, and 125 backward trajectories were identified for October 2021. These trajectories revealed three clusters, one of which represented a path followed by 61 % of clusters originating from Lake Superior and terminating in St. Louis. Another trajectory was traced by 23 % of clusters, commencing in the Pacific Ocean and following the Canadian-American border, ultimately reaching St. Louis from the northern United States. The last trajectory, accounting for 16 % of clusters, began in

Russia, traversed the Pacific Ocean, and arrived in St. Louis via the northwestern United States.

Figure 2.8 (b) presents the number of backward trajectories in November 2021. According to TSV, there were two clusters, and 121 backward trajectories were identified for November 2021. These trajectories represented two clusters. The first trajectory, followed by 50 % of clusters, originated near Russia in the Bering Sea, proceeded to Alaska, and then followed a pathway through Canada before reaching St. Louis. The second trajectory, also followed by 50% of clusters, commenced near Canada in the Pacific Ocean, traveled across Canada, and ultimately arrived in St. Louis.

Figure 2.8 (c) illustrates the number of backward trajectories in December 2021. According to TSV, four clusters were identified, with a total of 125 backward trajectories found for December 2021. These trajectories were grouped into four clusters. The first trajectory, followed by 17 % of the clusters, originated in northern Russia, traveled through southern Russia, then proceeded to St. Louis via a pathway through the Pacific Ocean and the northwestern United States. Another trajectory, followed by 32 % of the clusters, began near Alaska in the Pacific Ocean and traversed to St. Louis from the western United States. A third trajectory, followed by 34 % of the clusters, originated near Russia in the East Siberian Sea, passed over Alaska, and found a pathway through Canada before arriving in St. Louis from the northwestern United States. The last trajectory, representing 18% of the clusters, started from somewhere in the Gulf of Mexico and traversed to St. Louis from the southern United States. Table 2.8 provides information, including the number of trajectories, cluster percentages, starting locations, and directions for October, November, and December 2021.

Table 2.8 The number of trajectories, percentage of clusters, starting points and directions for October, November, and December 2021.

Month	Number of trajectories	Percentile of clusters	Starting location	Directions
October 2021	3	61 %	Lake Superior	the northeastern direction
		23 %	The Pacific Ocean	the northern direction
		16 %	Russia	the northwestern direction
November 2021	2	50 %	Russia	the northwestern direction
		50 %	near Canada in The Pacific Ocean	the northwestern direction
December 2021	4	17 %	Russia	the northwestern direction
		32 %	near Alaska in The Pacific Ocean	the western direction
		34 %	Russia	the northwestern direction
		18 %	Gulf of Mexico	the southern direction

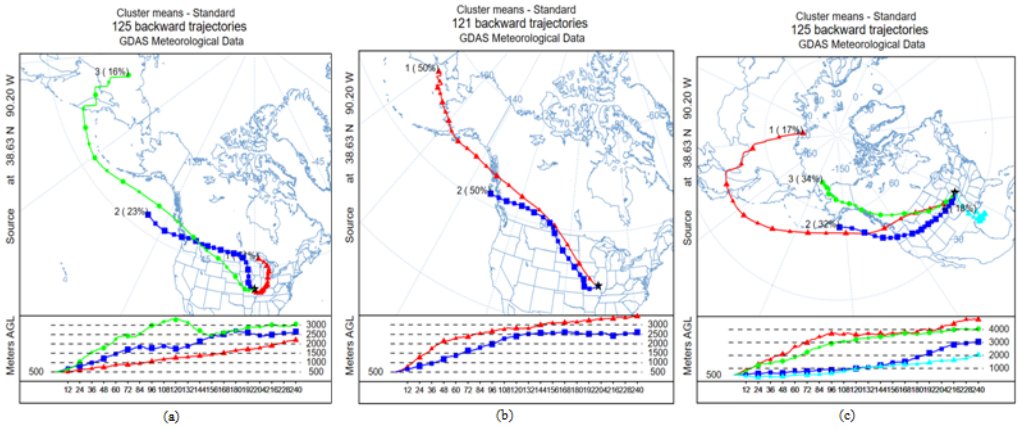

Figure 2.8 The number of backward trajectories (a) October 2021, (b) November 2021, (c) December 2021.

2.1.3. Backward Trajectory Analysis of Air Masses from January 2022 to December 2022 in St. Louis. Backward trajectory and cluster analysis were generated from January 2022 to December 2022 on the HYSPLIT modeling program. The calculation was made according to 240 total hours backward and 6-hour time intervals. In January 2022, Figure 2.9 (a) presents the data on the number of backward trajectories. According to TSV, these trajectories were classified into three clusters, with a total of 125 backward

trajectories identified for January 2022. These trajectories showcased three distinct clusters: the first, followed by 26 % of the clusters, originated from a point in Russia, proceeded through the Pacific Ocean and the western United States, and ultimately reached St. Louis from the northwestern United States. The second trajectory, representing 53 % of the clusters, initiated in the Pacific Ocean, transited through Canada, and culminated in St. Louis from the northwestern United States. The third trajectory, comprising 22 % of the clusters, commenced its journey in the Arctic Ocean, traversed through Canada, and concluded in St. Louis from the northern United States.

Figure 2.9 (b) displays the quantity of backward trajectories in February 2022. According to TSV, there were two clusters, and a total of 113 backward trajectories were identified for February 2022. Within the context of February 2022, these clusters exhibited distinct patterns. The first trajectory, representing 43 % of the clusters, originated in the vicinity of the Kuril Islands and traversed the Pacific Ocean, passing through Canada before reaching St. Louis. Conversely, the remaining trajectory, followed by 57 % of the clusters, had its origin in the Arctic Ocean, moved across Canada, and arrived in St. Louis from the northern United States.

Figure 2.9 (c) illustrates the quantity of backward trajectories in March 2022. According to TSV, there were three distinct clusters, and a total of 125 backward trajectories were identified for March 2022. Within the scope of March 2022, these clusters revealed unique characteristics. The first trajectory, representing 28 % of the clusters, initiated its path from the sea of Okhotsk, traversed the Pacific Ocean, passed through Canada, and reached St. Louis from the northwestern United States. The second trajectory, followed by 34 % of the clusters, had its starting point somewhere in Canada and traversed

to St. Louis. Lastly, the third trajectory, followed by 38 % of the clusters, originated from the Arctic Ocean, crossed Canada, and ultimately reached St. Louis from the northern United States. Table 2.9 provides information, including the number of trajectories, cluster percentages, starting locations, and directions for January, February, and March 2022.

Table 2.9 The number of trajectories, percentage of clusters, starting points and directions for January, February, and March 2022.

Month	Number of trajectories	Percentile of clusters	Starting location	Directions
January 2022	3	26 %	Russia	the northwestern direction
		53 %	The Pacific Ocean	the northwestern direction
		22 %	The Arctic Ocean	the northern direction
February 2022	2	43 %	Kuril Islands	the northern direction
		57 %	The Arctic Ocean	the northern direction
March 2022	3	28 %	The sea of Okhotsk	the northwestern direction
		34 %	Canada	the northwestern direction
		38 %	The Arctic Ocean	the northern direction

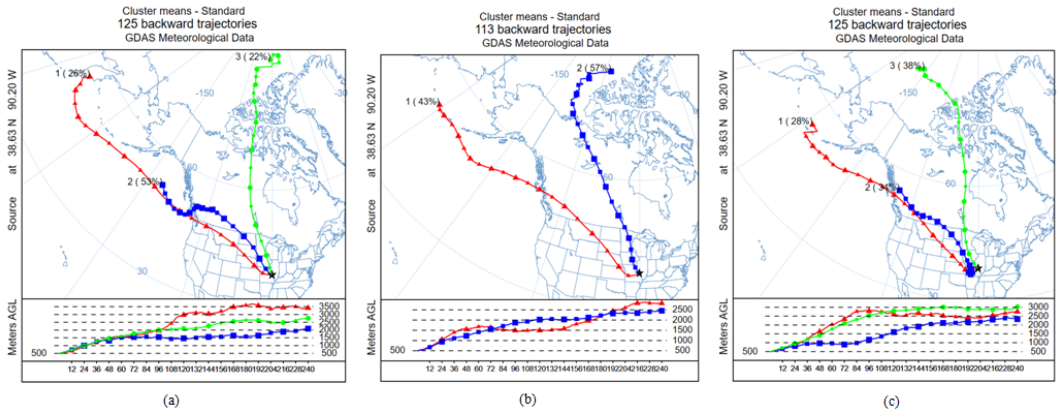

Figure 2.9 The number of backward trajectories (a) January 2022, (b) February 2022, (c) March 2022.

Figure 2.10 (a) depicts the quantity of backward trajectories in April 2022. As per TSV, there were two clusters identified, and a total of 121 backward trajectories were

discovered for April 2022. The trajectories exhibited two distinct clusters: one followed by 74 % of the clusters, commencing from a location in Canada and concluding its course in St. Louis, originating from the northern United States. The second trajectory was followed by 26 % of the clusters, with its starting point near the Kuril Islands in the Atlantic Ocean. It proceeded through the northwestern United States, passing through Washington, Idaho, Montana, Wyoming, Nebraska, and Kansas, before arriving in St. Louis. Table 2.10 provides information, including the number of trajectories, cluster percentages, starting locations, and directions for April, May, and June 2022.

Table 2.10 The number of trajectories, percentage of clusters, starting points and directions for April, May, and June 2022.

Month	Number of trajectories	Percentile of clusters	Starting location	Directions
April 2022	2	74 %	Canada	the northern direction
		26 %	Kuril Islands	the northwestern direction
May 2022	3	46 %	Canada	the northern direction
		18 %	The sea of Okhotsk	the northwestern direction
		36 %	The Pacific Ocean	the southern direction
June 2022	4	17 %	The Pacific Ocean	the northwestern direction
		22 %	The Atlantic Ocean	the southern direction
		34 %	Great Slave Lake in Canada	the northern direction
		27 %	Russia	the northern direction

Figure 2.10 (b) displays the quantity of backward trajectories in May 2022. Based on TSV, three clusters were identified, with a total of 125 backward trajectories observed for May 2022. These trajectories depicted three distinct clusters. The first trajectory was followed by 46 % of the clusters, originating from a location in Canada and concluding its path in St. Louis, stemming from the northern United States. The second trajectory, followed by 18 % of the clusters, commenced from a location in the Sea of Okhotsk and

proceeded through the Pacific Ocean. It traversed through Oregon, Idaho, Montana, South Dakota, and Iowa, ultimately reaching St. Louis from the northwestern United States. The third trajectory, followed by 36 % of the clusters, started in the Pacific Ocean and proceeded through the Gulf of Mexico. It followed a route through Mississippi and Arkansas before arriving in St. Louis from the southern United States.

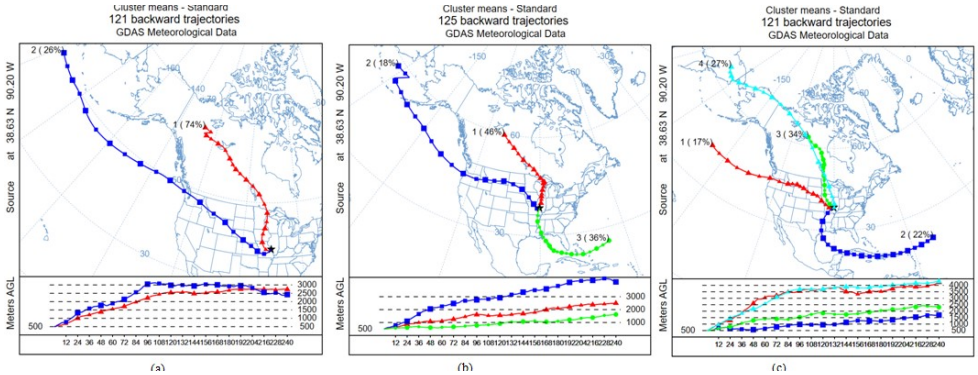

Figure 2.10 The number of backward trajectories (a) April 2022, (b) May 2022, (c) June 2022.

Figure 2.10 (c) presents the number of backward trajectories in June 2022. According to TSV, four clusters were identified, with a total of 121 backward trajectories documented for June 2022. These trajectories delineated four distinct clusters. The first trajectory, followed by 17 % of the clusters, initiated in the Pacific Ocean and passed through Oregon, traversing Idaho, Montana, Wyoming, South Dakota, and Nebraska, before culminating in St. Louis. Another trajectory, which constituted 22 % of the clusters, commenced from a location in the Atlantic Ocean. It journeyed through the Gulf of Mexico, followed a pathway through Texas, Oklahoma, and Arkansas, and eventually arrived in St. Louis from the southern United States. The third trajectory, accounting for 34 % of the clusters, began near the Great Slave Lake in Canada and reached St. Louis

from the northern United States. The final trajectory, followed by 27 % of the clusters, originated in Russia, traversed through Alaska and Canada, and concluded its path in St. Louis.

Figure 2.11 (a) depicts the number of backward trajectories in July 2022. Based on TSV, two distinct clusters were identified, and a total of 125 backward trajectories were recorded for July 2022. These trajectories encompassed two clusters. The first trajectory, constituting 71 % of the clusters, originated in the Pacific Ocean between Haida Gwaii Islands and Canada. It traversed through North Dakota, South Dakota, and Iowa, ultimately reaching St. Louis from the northwestern United States. The second trajectory, followed by 29 % of the clusters, commenced in the Atlantic Ocean. It extended its path over Cuba, utilizing a pathway through the Gulf of Mexico, Texas, and Arkansas, before culminating in St. Louis.

Figure 2.11 (b) displays the number of backward trajectories in August 2022. According to TSV, there were two distinct clusters identified, encompassing a total of 125 backward trajectories for August 2022. One of these clusters consisted of a trajectory followed by 34 % of the clusters, originating in the Atlantic Ocean, passing over the Gulf of Mexico, and concluding in St. Louis. The second trajectory, followed by 66 % of the clusters, initiated from the Great Slave Lake in Canada. It traversed through Minnesota, following a pathway through Wisconsin and Illinois, before arriving in St. Louis from the northern United States.

Figure 2.11 (c) depicts the number of backward trajectories in September 2022. According to TSV, there were two identified clusters, accounting for a total of 121 backward trajectories for September 2022. One of these clusters featured a trajectory

followed by 35 % of the clusters, commencing from the Andreanof Islands and traveling through the Pacific Ocean, utilizing a pathway through Canada, North Dakota, Minnesota, and Iowa, ultimately reaching St. Louis from the northwestern United States. The second trajectory, followed by 65 % of the clusters, had its origin in southern Canada and traversed through Michigan, Wisconsin, and Illinois before arriving in St. Louis from the northern United States. Table 2.11 provides information, including the number of trajectories, cluster percentages, starting locations, and directions for July, August, and September 2022.

Table 2.11 The number of trajectories, percentage of clusters, starting points and directions for July, August, and September 2022.

Month	Number of trajectories	Percentile of clusters	Starting location	Directions
July 2022	2	71 %	The Pacific Ocean	the northwestern direction
		29 %	The Atlantic Ocean	the southern direction
August 2022	2	34 %	The Atlantic Ocean	the southern direction
		66 %	Great Slave Lake in Canada	the northern direction
September 2022	2	35 %	Andreanof Islands	the northwestern direction
		65 %	Canada	the norhern direction

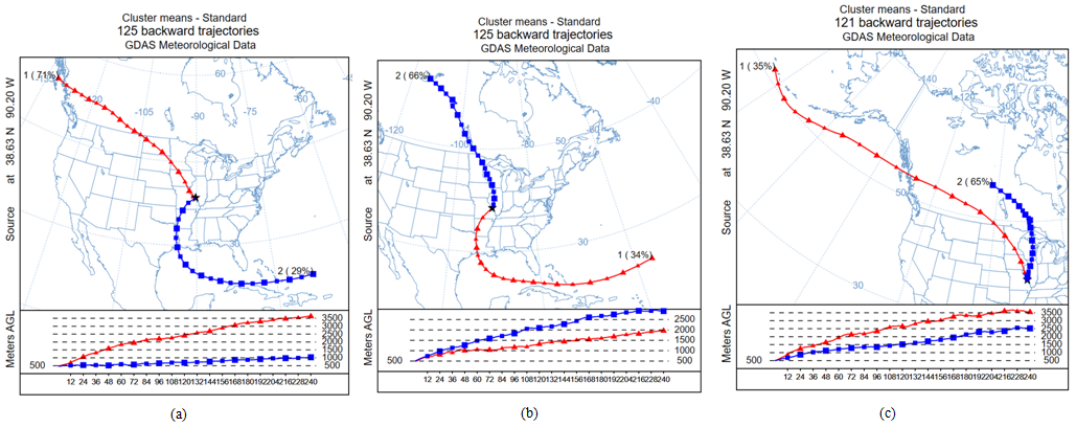

Figure 2.11 The number of backward trajectories (a) July 2022, (b) August 2022, (c) September 2022.

Figure 2.12 (a) illustrates the number of backward trajectories in October 2022. According to TSV, there were two clusters identified, with a total of 125 backward trajectories for October 2022. One of these clusters featured a trajectory followed by 48 % of the clusters, originating from southwestern Canada. This trajectory passed through North Dakota and followed a pathway through Minnesota and Iowa before reaching St. Louis. The second trajectory, followed by 52 % of the clusters, began in the East Siberian Sea and moved through Russia, utilizing a pathway through the Bering Strait, Alaska, and Canada, ultimately arriving in St. Louis from the northern United States.

Figure 2.12 (b) presents the number of backward trajectories in November 2022. According to TSV, there were two clusters identified, with a total of 121 backward trajectories for November 2022. In one cluster, the trajectory was followed by 62 % of the clusters and began in southwestern Canada. It passed through North Dakota and followed a pathway through South Dakota and Iowa before arriving in St. Louis. In the other cluster, followed by 38 % of the clusters, the trajectory originated in Russia and traveled through the Bering Strait, utilizing a pathway through Alaska and Canada, before reaching St. Louis from the northwestern United States.

Figure 2.12 (c) displays the number of backward trajectories in December 2022. According to TSV, three clusters were identified, totaling 125 backward trajectories for December 2022. In one of the clusters, followed by 61 % of the trajectories, the trajectory originated in southwestern Canada and passed through Washington. It followed a pathway through Idaho, Montana, Wyoming, Nebraska, and traversed to St. Louis from the northwestern United States. Another trajectory, followed by 26 % of the clusters, began in Russia and traveled over the Bering Sea. It continued through Alaska and followed a

pathway through Canada, North Dakota, South Dakota, and Nebraska before reaching St. Louis from the northwestern United States. The last trajectory, followed by 14 % of the clusters, commenced in the middle of Greenland. It traversed through the Labrador Sea and passed through the Gulf of Hudson. This trajectory found a pathway through Canada, Minnesota, and Iowa before arriving in St. Louis from the northern United States. Table 2.12 provides information, including the number of trajectories, cluster percentages, starting locations, and directions for October, November, and December 2022.

Table 2.12 The number of trajectories, percentage of clusters, starting points and directions for October, November, and December 2022.

Month	Number of trajectories	Percentile of clusters	Starting location	Directions
October 2022	2	48 %	Canada	the northern direction
		52 %	The East Siberian Sea	the northern direction
November 2022	2	62 %	Canada	the northwestern direction
		38 %	Russia	the northwestern direction
December 2022	3	61 %	Canada	the northwestern direction
		26 %	Russia	the northwestern direction
		14 %	Greenland	the northern direction

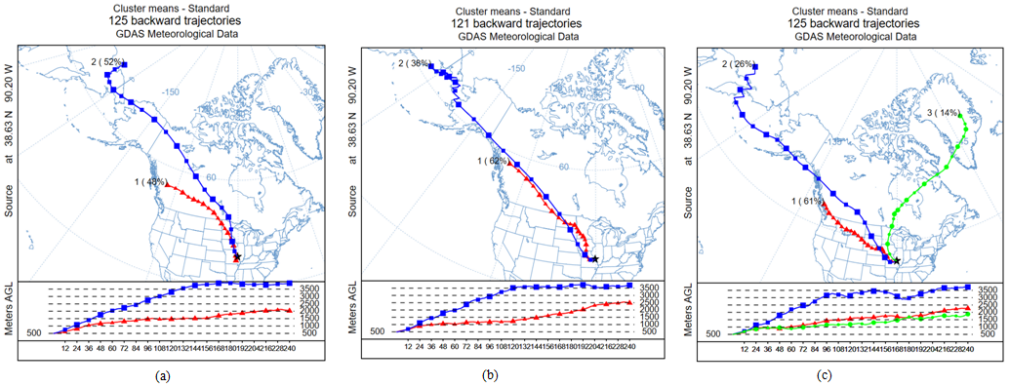

Figure 2.12 The number of backward trajectories (a) October 2022, (b) November 2022, (c) December 2022.

2.2. SEASONAL BACKWARD TRAJECTORY ANALYSIS OF AIR MASS IN ST. LOUIS

Backward trajectory and cluster analysis are done seasonally for autumn, winter, spring, and summer for 2020, 2021 and 2022.

2.2.1. Seasonal Backward Trajectory Analysis of Air Mass in St. Louis for 2020. Backward trajectory and cluster analysis are conducted seasonally for autumn, winter, spring, and summer 2020. Figure 2.13 (a) illustrates the number of backward trajectories in autumn 2020. According to TSV, three clusters were identified, totaling 364 backward trajectories for autumn 2020. In one of the clusters, followed by 58 % of the trajectories, the trajectory began near Russia in the Sea of Okhotsk and traveled through the Bering Sea, following a pathway through Alaska and Canada before reaching St. Louis from the northwestern United States. Another trajectory, followed by 33 % of the clusters, originated in southern Canada and moved directly to St. Louis. The last trajectory, followed by 9 % of the clusters, started from Svalbard Island and traveled over the Arctic Ocean. It followed a pathway through the Beaufort Sea and Canada before arriving in St. Louis.

Figure 2.13 (b) displays the number of backward trajectories in winter 2020. According to TSV, two clusters were identified, totaling 365 backward trajectories for winter 2020. Within the winter season, two clusters were observed. The first cluster, consisting of 61 % of the trajectories, originated from a location in Russia and followed a path through the Sea of Okhotsk. It continued through Alaska and Canada before reaching St. Louis from the northwestern United States. The second trajectory, followed by 39 % of the clusters, began in the Pacific Ocean. It passed over Washington and followed a pathway through Idaho, Montana, North Dakota, South Dakota, and Nebraska on its way to St. Louis from the northwestern United States. Table 2.13 provides information, including the

number of trajectories, cluster percentages, starting locations, and directions for Autumn and Winter 2020.

Table 2.13 The number of trajectories, percentage of clusters, starting points and directions for Autumn and Winter 2020.

Month	Number of trajectories	Percentile of clusters	Starting location	Directions
Autumn 2020	3	58 %	The sea of Okhotsk	the northwestern direction
		33 %	Canada	the northwestern direction
		9 %	Svalbard Island	the northwestern direction
Winter 2020	2	61 %	Russia	the northwestern direction
		39 %	The Pacific Ocean	the northwestern direction

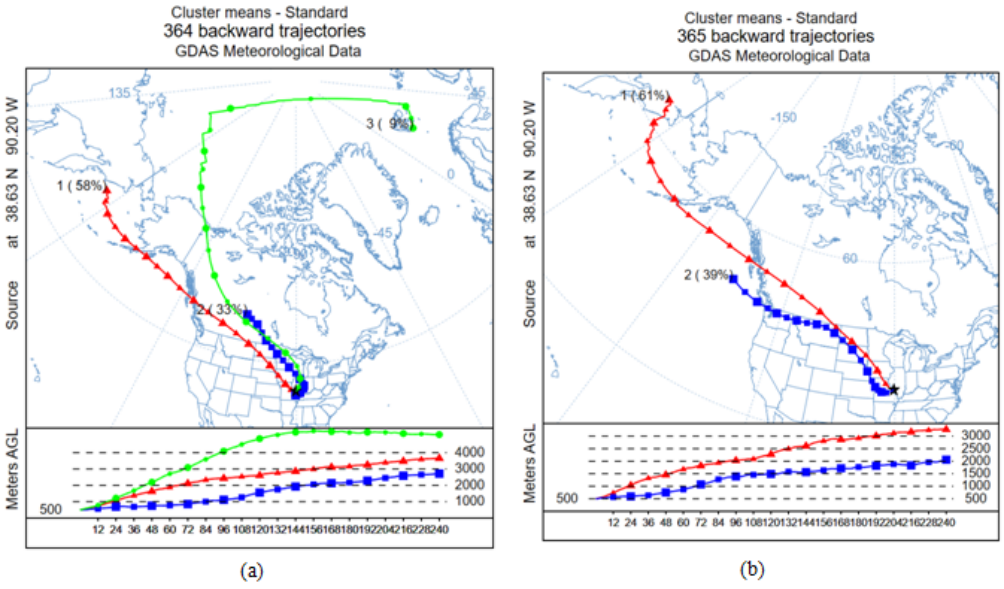

Figure 2.13 The number of backward trajectories (a) Autumn 2020, (b) Winter 2020.

Figure 2.14 (a) displays the number of backward trajectories in spring 2020. According to TSV, two clusters were identified, totaling 368 backward trajectories for spring 2020. Within the spring season, two clusters were observed. The first cluster, consisting of 37 % of the trajectories, originated from a location near the Sea of Okhotsk.

It followed a path through the Kuril Islands and the Gulf of Alaska, then continued through Canada, North Dakota, Minnesota, and Iowa before reaching St. Louis. The second trajectory, followed by 63 % of the clusters, began in South Canada and followed a pathway through North Dakota, Minnesota, and Iowa on its way to St. Louis. Table 2.14 provides information, including the number of trajectories, cluster percentages, starting locations, and directions for Spring and Summer 2020.

Table 2.14 The number of trajectories, percentage of clusters, starting points and directions for Spring and Summer 2020.

Month	Number of trajectories	Percentile of clusters	Starting location	Directions
Spring 2020	2	37 %	The sea of Okhotsk	the northwestern direction
		63 %	Canada	the northwestern direction
Summer 2020	2	61 %	Canada	the northwestern direction
		39 %	The Atlantic Ocean	the southern direction

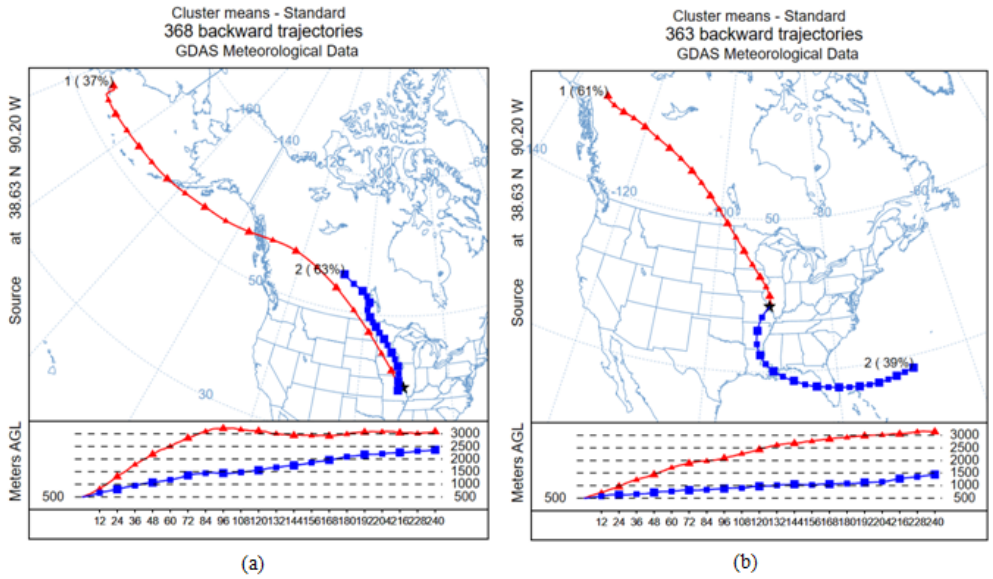

Figure 2.14 The number of backward trajectories (a) Spring 2020, (b) Summer 2020.

Figure 2.14 (b) presents the number of backward trajectories for summer 2020. According to TSV, two clusters were identified, totaling 363 backward trajectories for the summer season. In summer, two distinct clusters were observed. The first trajectory, followed by 61 % of the clusters, originated from a location in Canada and followed a path through North Dakota, Minnesota, Iowa, and Illinois before reaching St. Louis from the northwestern United States. The second trajectory, followed by 39 % of the clusters, began in the Atlantic Ocean. It passed over Florida and took a route through the Gulf of Mexico, Louisiana, and Arkansas on its way to St. Louis from the southern United States.

2.2.2. Seasonal Backward Trajectory Analysis of Air Mass in St. Louis for 2021. Backward trajectory and cluster analysis are done seasonally for autumn, winter, spring, and summer 2021. Figure 2.15 (a) illustrates the number of backward trajectories for autumn 2021. Based on TSV, four clusters were identified, totaling 365 backward trajectories for the autumn season. In autumn 2021, four distinct clusters were observed. The first trajectory, followed by 39 % of the clusters, originated in the Pacific Ocean near Alaska, passed through Canada, and concluded in St. Louis. The second trajectory, followed by 17 % of the clusters, began in South Carolina, traveled through Florida, and found a pathway through Alabama and Tennessee before reaching St. Louis. Another trajectory, followed by 27 % of the clusters, started somewhere in Canada and traversed to St. Louis. The final trajectory, followed by 18 % of the clusters, began in Russia and followed a path through Alaska and Canada to reach St. Louis.

Figure 2.15 (b) shows the number of backward trajectories in winter 2021. According to TSV, the number of clusters was two, and 361 backward trajectories were found for winter. There were two clusters in winter 2021, one of which was a trajectory

followed by 52 % of clusters started from somewhere in Russia and took a pathway through Alaska and Canada and moved to St. Louis, and the last trajectory followed by 48 % of clusters starting from somewhere in Canada and traveled to St. Louis. Table 2.15 provides information, including the number of trajectories, cluster percentages, starting locations, and directions for Autumn and Winter 2021.

Table 2.15 The number of trajectories, percentage of clusters, starting points and directions for Autumn and Winter 2021.

Month	Number of trajectories	Percentile of clusters	Starting location	Directions
Autumn 2021	4	39 %	The Pacific Ocean	the northwestern direction
		17 %	South Carolina	the southern direction
		27 %	Canada	the northern direction
		18 %	Russia	the northwestern direction
Winter 2021	2	52 %	Russia	the northwestern direction
		48 %	Canada	the northwestern direction

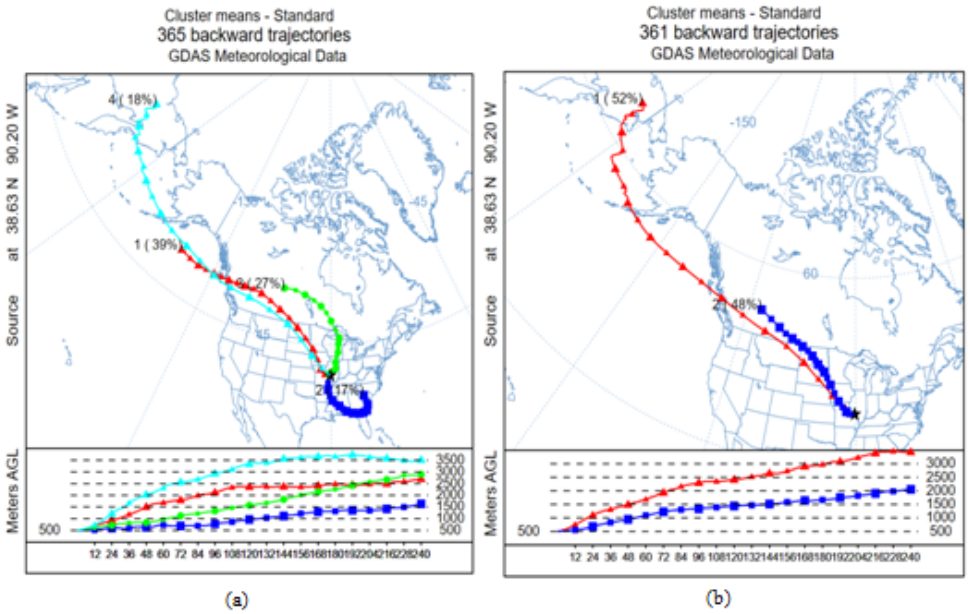

Figure 2.15 The number of backward trajectories (a) Autumn 2021, (b) Winter 2021.

Figure 2.16 (a) shows the number of backward trajectories in spring 2021. According to TSV, the number of clusters was three, and 369 backward trajectories were found for spring. There were three clusters in spring 2021, one of which was a trajectory followed by 23 % of clusters started from the Pacific Ocean and traversed to St. Louis, another trajectory followed by 31 % of clusters started from somewhere in Russia and found a pathway through Alaska and Canada and moved to St. Louis, and the last trajectory followed by 46 % of clusters started from somewhere in Gulf of Hudson and moved over through Canada and traveled to St. Louis. Table 2.16 provides information, including the number of trajectories, cluster percentages, starting locations, and directions for Spring and Summer 2021.

Table 2.16 The number of trajectories, percentage of clusters, starting points and directions for Spring and Summer 2021.

Month	Number of trajectories	Percentile of clusters	Starting location	Directions
Spring 2021	3	23 %	The Pacific Ocean	the northwestern direction
		31 %	Russia	the northwestern direction
		46 %	Gulf of Hudson	the northeastern direction
Summer 2021	3	38 %	Alaska	the northwestern direction
		35 %	North Dakota	the northwestern direction
		27 %	The Atlantic Ocean	the southern direction

Figure 2.16 (b) shows the number of backward trajectories in summer 2021. According to TSV, the number of clusters was three, and 369 backward trajectories were found for summer 2021. The number of backward trajectories in summer showed three clusters, one of which was a trajectory followed by 38 % of clusters starting from Alaska and moved through Canada and took a route to St. Louis through Canada, another trajectory followed by 35 % of clusters started from North Dakota to St. Louis from the northwestern

United States. The last trajectory followed by 27 % of clusters started from the Atlantic Ocean and traversed through the Gulf of Mexico through Louisiana and took a pathway to St. Louis through Arkansas.

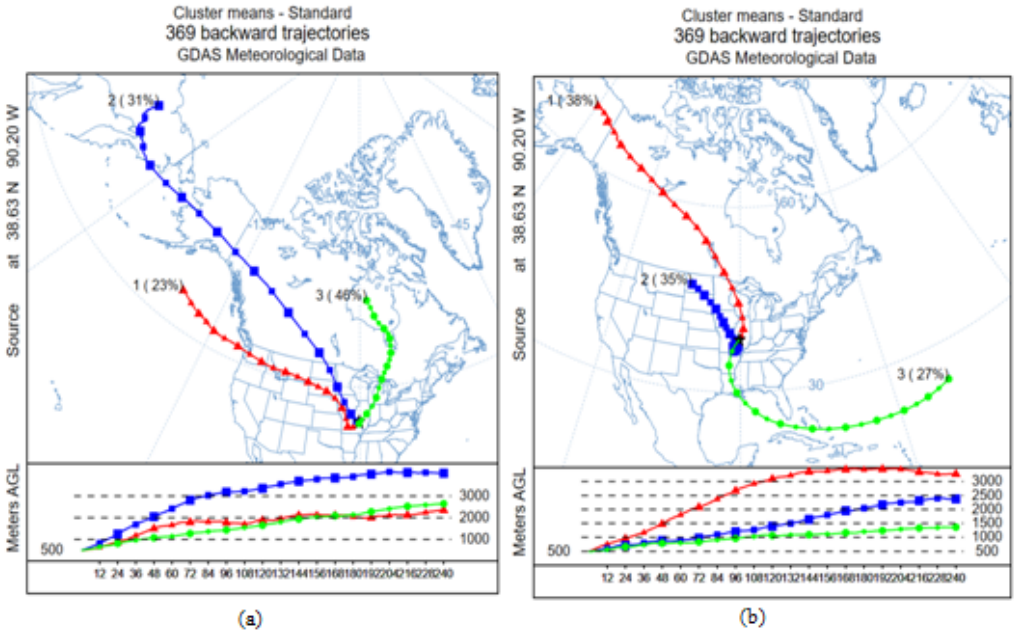

Figure 2.16 The number of backward trajectories (a) Spring 2021, (b) Summer 2021.

2.2.3. Seasonal Backward Trajectory Analysis of Air Mass in St. Louis for 2022. Backward trajectory and cluster analysis are done seasonally for autumn, winter, spring, and summer 2022. Figure 2.17 (a) shows the number of backward trajectories in autumn 2022. According to TSV, the number of clusters was two, and 365 backward trajectories were found for autumn 2022. The number of backward trajectories in autumn showed two clusters, one of which was a trajectory followed by 59 % of clusters started from somewhere in Canada through Minnesota, and Iowa and moved to St. Louis from the northern United States, and the last trajectory followed by 41 % of clusters started from somewhere in Russia and traversed through Bering Strait and found a pathway through

Alaska, Canada, Minnesota, Iowa and moved to St. Louis from the northern United States. Table 2.17 provides information, including the number of trajectories, cluster percentages, starting locations, and directions for Autumn and Winter 2022.

Table 2.17 The number of trajectories, percentage of clusters, starting points and directions for Autumn and Winter 2022.

Month	Number of trajectories	Percentile of clusters	Starting location	Directions
Autumn 2022	2	59 %	Canada	the northern direction
		41 %	Russia	the northern direction
Winter 2022	3	52 %	Canada	the northwestern direction
		25 %	Russia	the northwestern direction
		23 %	Greenland	the norhtern direction

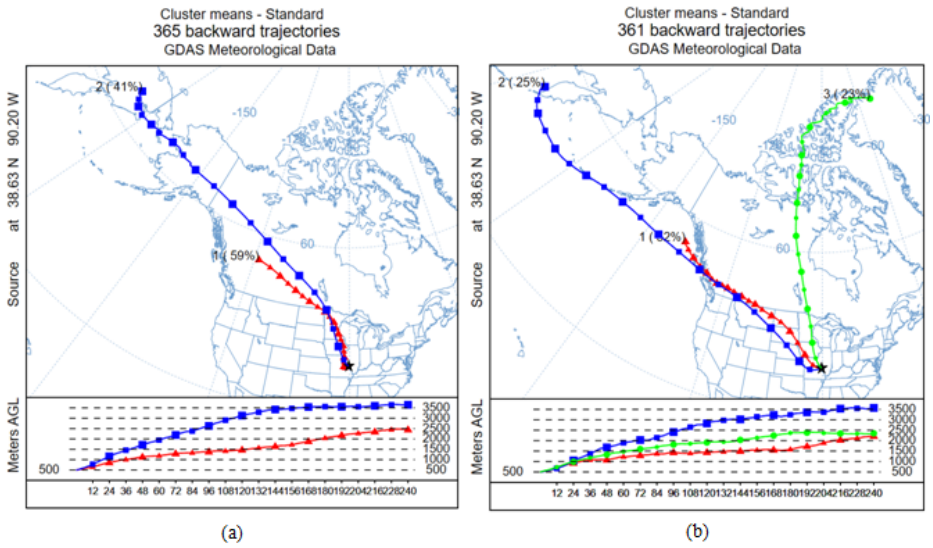

Figure 2.17 The number of backward trajectories (a) Autumn 2022, (b) Winter 2022.

Figure 2.17 (b) shows the number of backward trajectories in winter 2022. According to TSV, the number of clusters was three, and 361 backward trajectories were found for winter 2022. The number of backward trajectories in winter showed three clusters, one of which was a trajectory followed by 52 % of clusters started from

somewhere near Canada in the Pacific Ocean and traversed through Canada using pathway through Montana, North Dakota, South Dakota, Iowa and moved to St. Louis from the north west United States, and another trajectory followed by 25 % of clusters started from somewhere near Russia in the sea of Okhotsk and moved over through Bering Sea and found a pathway through the Pacific Ocean, Canada, Montana, South Dakota, Nebraska, Kansas and traveled to St. Louis from the north west United States, and the last trajectory followed by 23 % of clusters started from Greenland and moved through Queen Elizabeth Islands, and found a pathway through Canada, Minnesota, Iowa and moved to St. Louis from the north United States.

Figure 2.18 (a) shows the number of backward trajectories in spring 2022. According to TSV, the number of clusters was two, and 369 backward trajectories were found for spring 2022. The number of backward trajectories in spring showed two clusters, one of which was a trajectory followed by 55 % of clusters started from somewhere in south of Canada through Minnesota, Wisconsin, and Illinois and moved to St. Louis, and the last trajectory followed by 45 % of clusters started from somewhere in Russia and traveled through Alaska, and found a pathway through Canada, North Dakota, South Dakota, and Iowa and moved to St. Louis from the north west United States.

Figure 2.18 (b) shows the number of backward trajectories in summer 2022. According to TSV, the number of clusters was three, and 369 backward trajectories were found for summer 2022. The number of backward trajectories in summer showed three clusters, one of which was a trajectory followed by 52 % of clusters started from somewhere in Canada and moved through Minnesota, Iowa and traveled to St. Louis from the north west United States, and another trajectory followed by 19 % of clusters started

from somewhere near Russia in Bering Sea and traversed through Alaska, and found a pathway through Canada, Minnesota, Iowa and moved to St. Louis from the north west United States, and the last trajectory followed by 29 % of clusters started from somewhere in the Atlantic Ocean and moved over through Cuba, and took a pathway through the Gulf of Mexico, Texas, Arkansas and traveled to St. Louis from the southern United States. Table 2.18 provides information, including the number of trajectories, cluster percentages, starting locations, and directions for Spring and Summer 2022.

Table 2.18 The number of trajectories, percentage of clusters, starting points and directions for Spring and Summer 2022.

Month	Number of trajectories	Percentile of clusters	Starting location	Directions
Spring 2022	2	55 %	Canada	the northeastern direction
		45 %	Russia	the northwestern direction
Summer 2022	3	52 %	Canada	the northwestern direction
		19 %	near Russia in Bering Sea	the northwestern direction
		29 %	The Atlantic Ocean	the southern direction

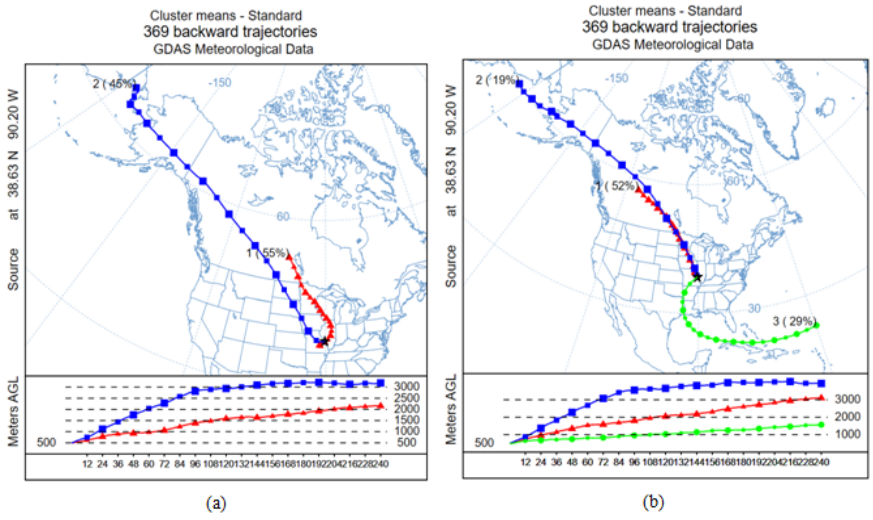

Figure 2.18 The number of backward trajectories (a) Spring2022, (b) Summer 2022.

3. AIR QUALITY DATA ANALYSIS FOR ST. LOUIS IN 2020, 2021, AND 2022

St. Louis is the second-largest city in Missouri and is located on the Mississippi River in the east-central region of the state. As per the U.S. Census Bureau Population Estimates Program (PEP), the estimated population of St. Louis was 300,483 in 2020, 293,310 in 2021, and 286,578 in 2022. To examine the air quality in the city, we analyzed the data collected by the air quality sensors installed by the Environmental Protection Agency for the years 2020, 2021, and 2022. St. Louis has always been a significant trading bridge between the east and the west due to its strategic location and well-connected transit lines. Additionally, its proximity to major rivers has facilitated the growth of marine transportation. The city is also home to several prominent industrial facilities.

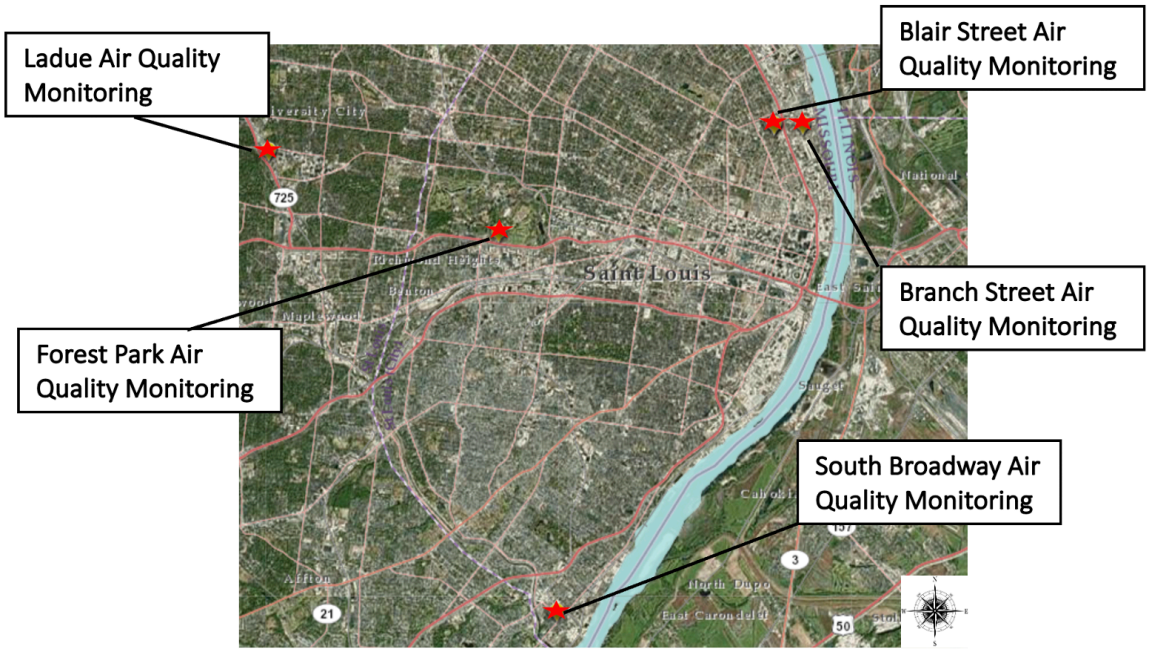

Figure 3.1 Air quality stations in St. Louis, Missouri.

According to the Environmental Protection Agency (EPA), the air quality in St. Louis, Missouri is monitored by five air quality monitors, namely Branch Street, Blair Street, Forest Park, Ladue, and South Broadway, as indicated in Figure 3.1. The highest arithmetic means of the pollutants measured by these monitors in the years 2020, 2021, and 2022 are calculated by the EPA. The tapered element oscillating microbalance (TEOM) instrument is used to measure the real-time particulate matter (PM) in the air. The TEOM can analyze up to five measurements per second to track the PM generation from engines (23).

3.1. $PM_{2.5}$ CONCENTRATION

According to the graph in Figure 3.2, all the Air Quality Monitors in St. Louis recorded their highest arithmetic mean in July 2020. The annual average $PM_{2.5}$ concentration for 2020 in St. Louis was 8.23 $\mu g/m^3$, as per the data presented. The EPA National Ambient Air Quality Standards have set the annual average of $PM_{2.5}$ concentration for primary and secondary standards at 12.0 $\mu g/m^3$ and 15.0 $\mu g/m^3$, respectively. According to the graph, it can be observed that the highest arithmetic mean was recorded by all the Air Quality Monitors in St. Louis in the month of July. Additionally, as depicted in Figure 3.3, the annual average concentration of $PM_{2.5}$ in St. Louis for the year 2021 is 8.525 $\mu g/m^3$. Based on the graph, it can be observed that the highest arithmetic mean recorded by all the Air Quality Monitors in St. Louis was in June 2022. Furthermore, as illustrated in Figure 3.4, the annual average concentration of $PM_{2.5}$ in St. Louis for the year 2022 is 7.66 $\mu g/m^3$. It can be observed that the highest concentration of $PM_{2.5}$ occurred in July for the years 2020 and 2021, and peaked in June for the year 2022. Typically, the

sources of $PM_{2.5}$ concentrations are industrial and combustion sources, as well as motor vehicle emissions (24). Additionally, the study indicated that the celebrations and fireworks on the Fourth of July led to an increase in the concentration of $PM_{2.5}$ in the air.

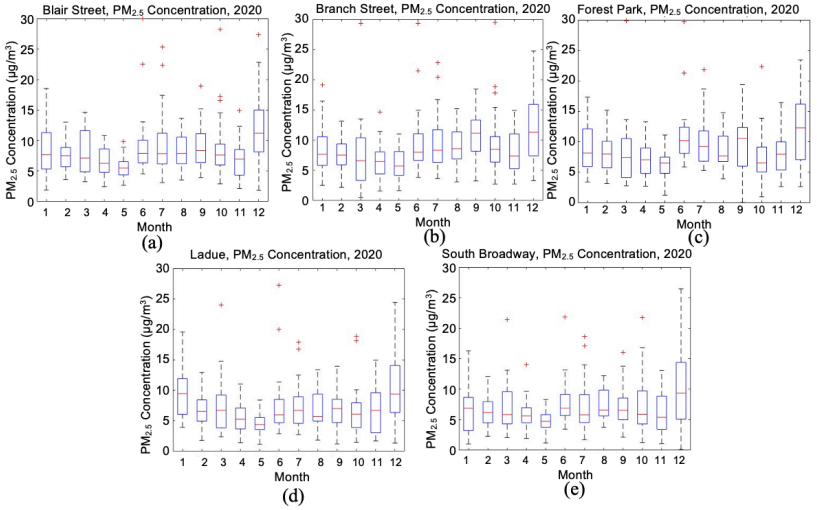

Figure 3.2 The graph of $PM_{2.5}$ concentration in 2020 for a) Blair Street, b) Branch Street, c) Forest Park, d) Ladue, e) South Broadway.

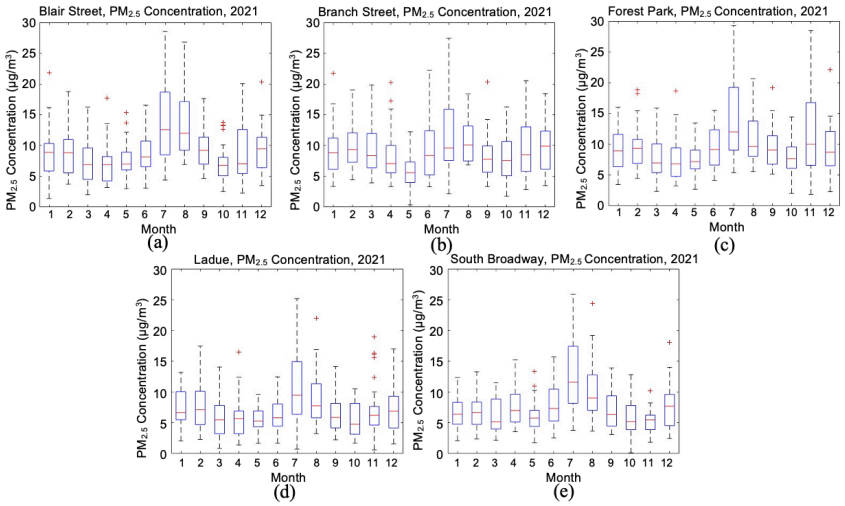

Figure 3.3 The graph of $PM_{2.5}$ concentration in 2021 for a) Blair Street, b) Branch Street, c) Forest Park, d) Ladue, e) South Broadway.

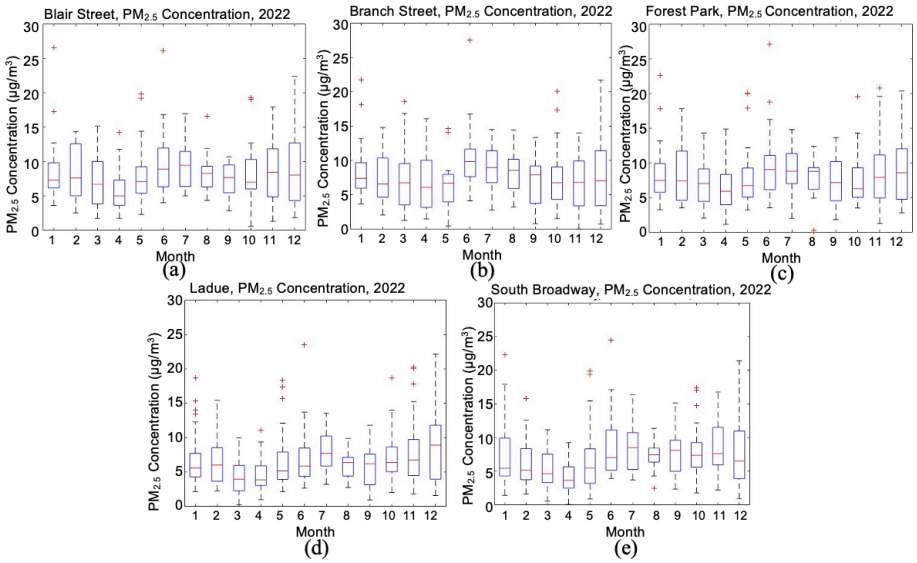

Figure 3.4 The graph of $PM_{2.5}$ concentration in 2022 for a) Blair Street, b) Branch Street, c) Forest Park, d) Ladue, e) South Broadway.

3.2. CARBON MONOXIDE CONCENTRATION

According to the graph in Figure 3.5, all the Air Quality Monitors in St. Louis recorded their highest arithmetic mean in December 2020. The annual average carbon monoxide (CO) concentration for 2020 in St. Louis was 0.252 parts per million (ppm), as per the data presented. The EPA National Ambient Air Quality Standards have set the annual average CO concentration for one hour at 35 ppm. According to the graph in Figure 3.6, all the Air Quality Monitors in St. Louis recorded their highest arithmetic mean in November 2021. As per the data presented, the annual average CO concentration for 2021 in St. Louis was 0.263 ppm. According to the graph in Figure 3.7, all the Air Quality Monitors in St. Louis recorded their highest arithmetic mean in November 2022. As per the data presented, the annual average CO concentration for 2022 in St. Louis was 0.245 ppm. As per the study findings, the highest concentration of CO was in December for the

year 2020, while it peaked in November for the years 2021 and 2022. CO concentrations in the atmosphere are mainly caused by heating, motor vehicles, and fuel and energy-related industries (25).

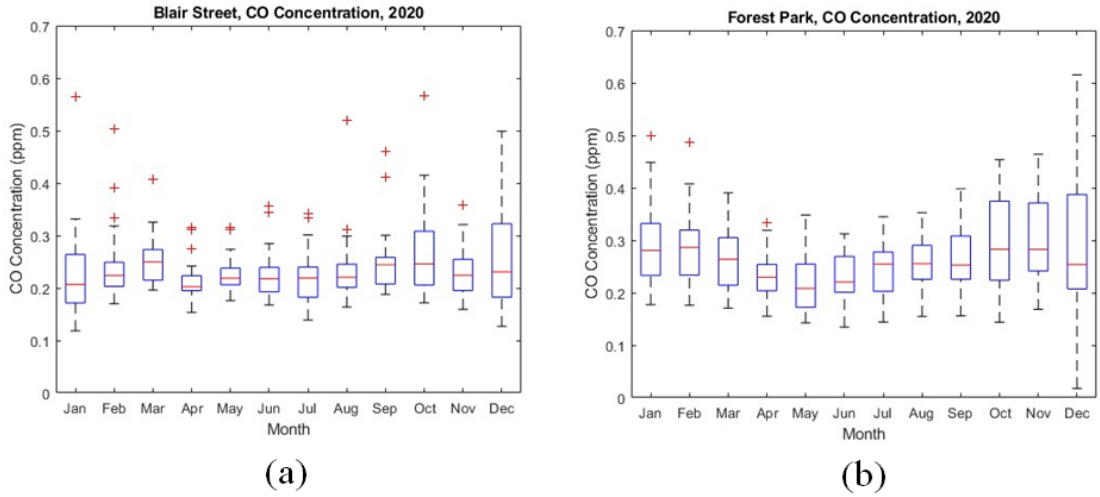

Figure 3.5 The graph of CO concentration in 2020 for a) Blair Street, b) Forest Park.

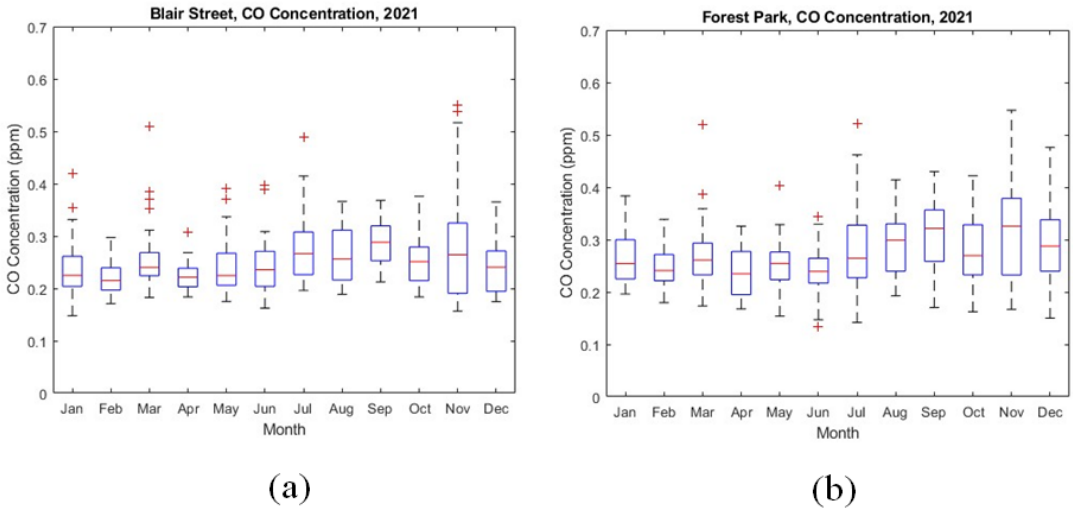

Figure 3.6 The graph of CO concentration in 2021 for a) Blair Street, b) Forest Park.

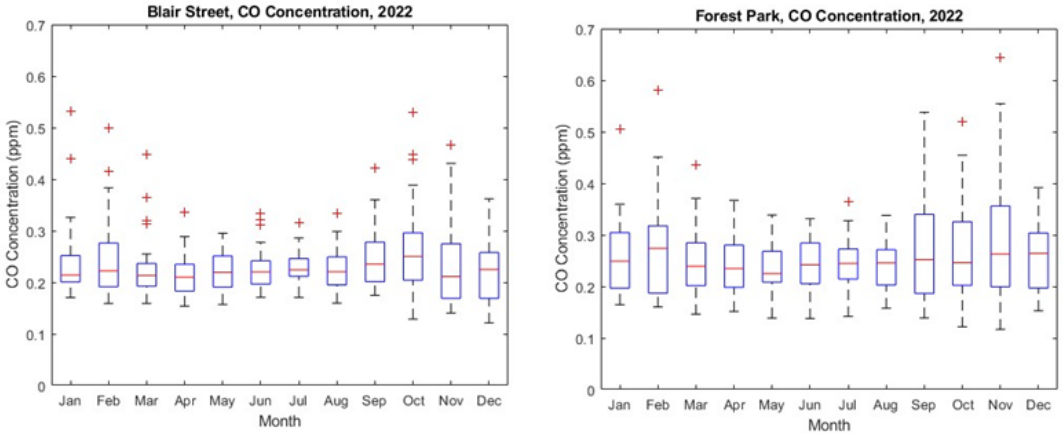

Figure 3.7 The graph of CO concentration in 2022 for a) Blair Street, b) Forest Park.

3.3. NITROGEN DIOXIDE CONCENTRATION

According to the graph in Figure 3.8, the Forest Park and Blair Street Air Quality Monitors in St. Louis had their highest recorded arithmetic mean in December 2020. In St. Louis, the annual average NO_2 concentration for 2020 was 9.540 parts per billion (ppb), as per the data presented. The EPA National Ambient Air Quality Standards have set the annual NO_2 concentration for primary and secondary standards at 53 ppb. According to the graph in Figure 3.9, the Forest Park and Blair Street Air Quality Monitors in St. Louis had their highest recorded arithmetic mean in March. As per the data presented, the annual average NO_2 concentration for 2021 in St. Louis was 9.720 ppb.

According to the graph in Figure 3.10, the Forest Park and Blair Street Air Quality Monitors in St. Louis had their highest recorded arithmetic mean in February 2022. As per the data presented, the annual average NO_2 concentration for 2022 in St. Louis was 9.163 ppb.

Based on the study findings, NO_2 concentrations peaked in December 2020, March 2021, and February 2022. It has been revealed that the majority of the increase in NO_2 concentrations is due to emissions from automobiles and industrial activities in industrial plants (26).

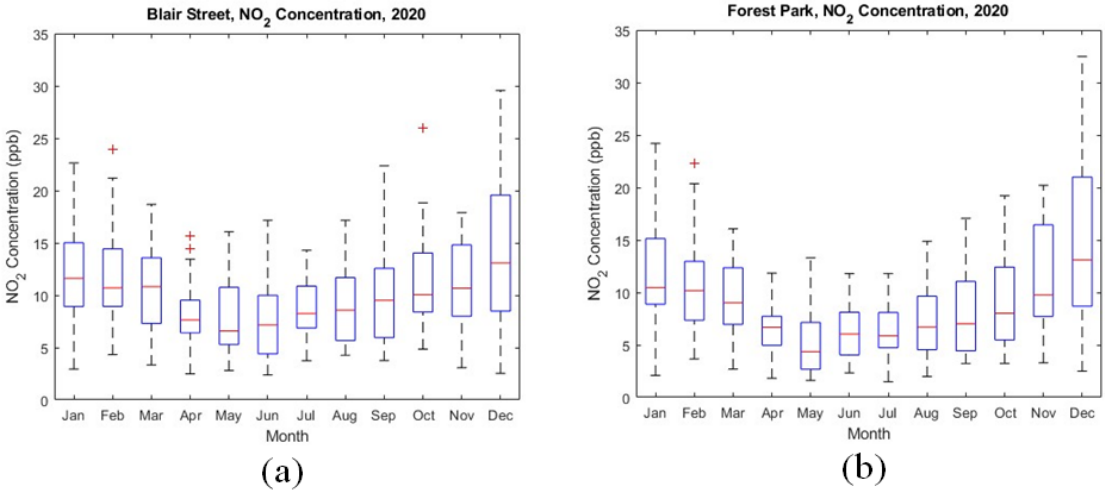

Figure 3.8 The graph of NO_2 concentration in 2020 for a) Blair Street, b) Forest Park.

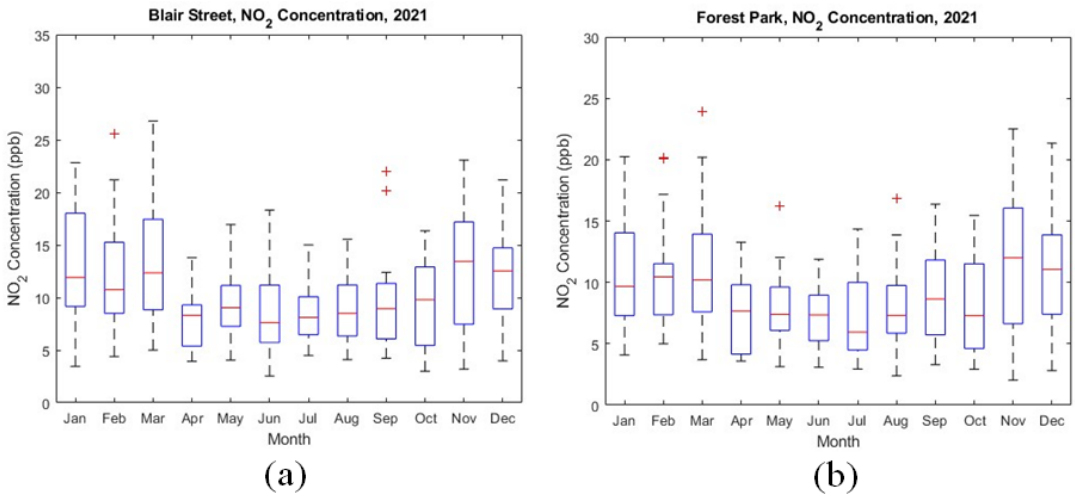

Figure 3.9 The graph of NO_2 concentration in 2021 for a) Blair Street, b) Forest Park.

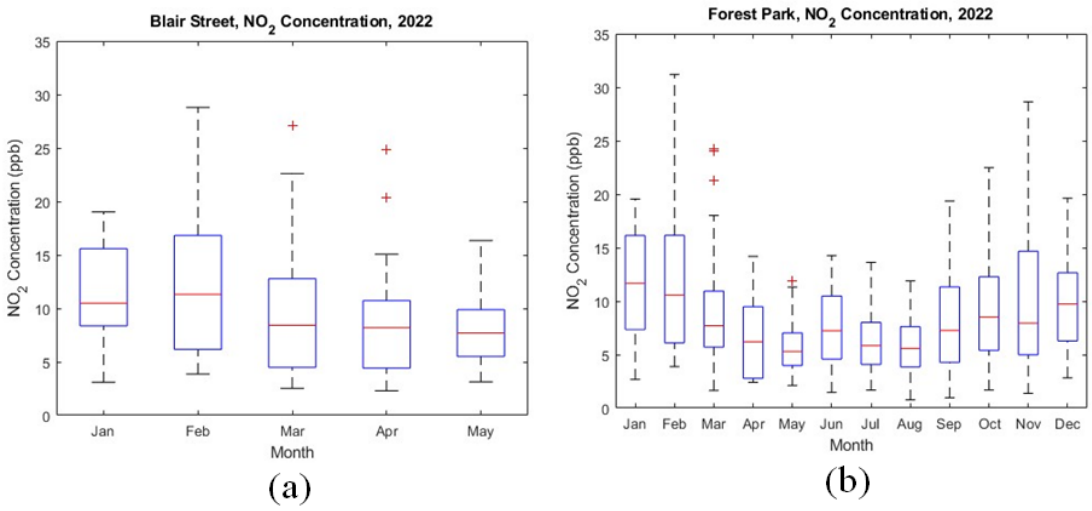

Figure 3.10 The graph of NO_2 concentration in 2022 for a) Blair Street, b) Forest Park.

3.4. NITRIC OXIDE CONCENTRATION

Based on the graph, it seems that both the Blair Street and Forest Park Air Quality Monitors in St. Louis recorded their highest arithmetic mean in December of 2020. As depicted in Figure 3.11, the annual average nitric oxide concentration for the year 2020 in St. Louis was 4.484 parts per billion (ppb). The NAAQS (National Ambient Air Quality Standards) for NO specifies a 1-hour standard at a level of 100 ppb and an annual standard at a level of 53 ppb, based on the 3-year average of the annual distribution of 1-hour maximum daily concentrations. According to the graph, it seems that the Blair Street Air Quality Monitor in St. Louis recorded its highest arithmetic mean in November, while the Forest Park Air Quality Monitor in St. Louis recorded its highest arithmetic mean in December. As shown in Figure 3.12, the annual average NO concentration for the year 2021 in St. Louis was 4.086 ppb. Based on the graph, it appears that the Blair Street Air Quality Monitor in St. Louis recorded its highest arithmetic mean in January 2022, while

the Forest Park Air Quality Monitor in St. Louis recorded its highest arithmetic mean in February 2022. As shown in Figure 3.13, the annual average NO concentration for the year 2022 in St. Louis was 3.791 ppb. It seems that the highest concentrations of NO were detected in December 2020, November and December 2021, and January and February 2022, as per the data. The emission of NO from motor vehicles and industrial facilities is known to increase their concentration in the air (26).

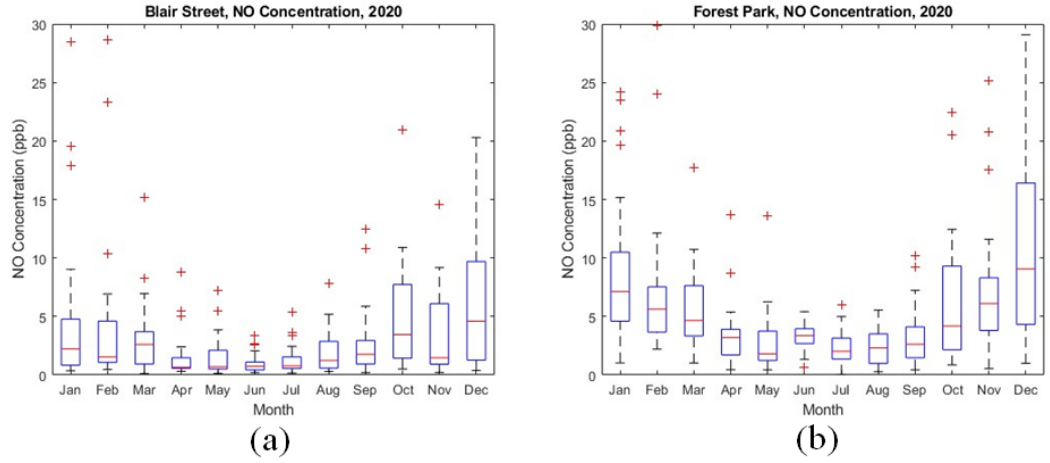

Figure 3.11 The graph of NO concentration in 2020 for a) Blair Street, b) Forest Park.

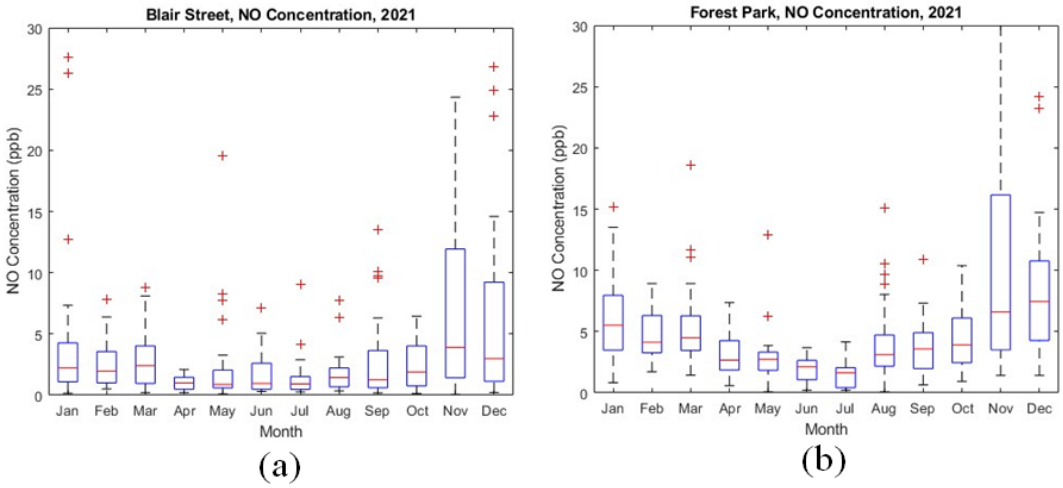

Figure 3.12 The graph of NO concentration in 2021 for a) Blair Street, b) Forest Park.

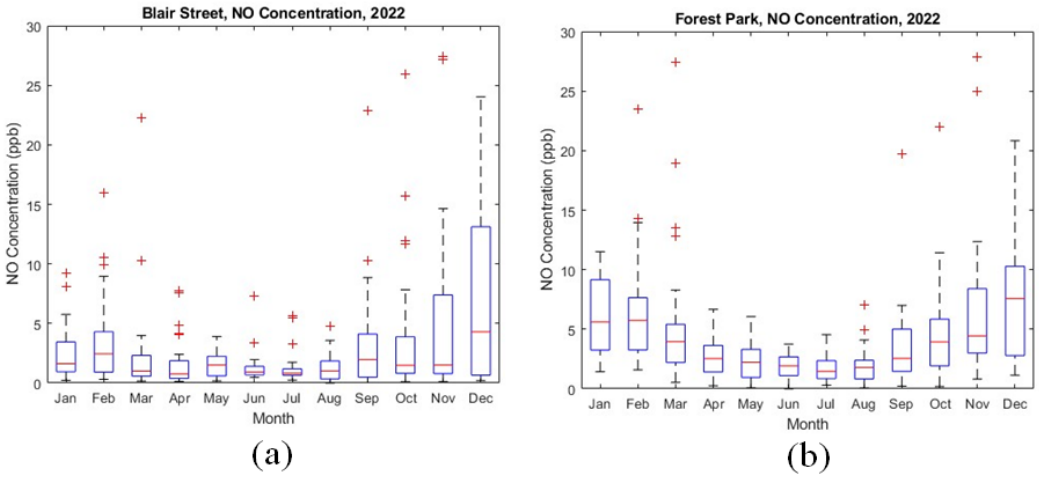

Figure 3.13 The graph of NO concentration in 2022 for a) Blair Street, b) Forest Park.

3.5. LEAD CONCENTRATION

Based on the graph, it appears that the Blair Street Air Quality Monitor in St. Louis experienced its highest arithmetic mean in December of 2020. As depicted in Figure 3.14, the average lead (Pb) concentration for the year 2021 in St. Louis was 0.006 micrograms/cubic per meter ($\mu g/m^3$). The EPA National Ambient Air Quality Standards specify an annual average of lead concentration for 3-month average primary and secondary standards to be 0.15 $\mu g/m^3$. Based on the graph, it appears that the Blair Street Air Quality Monitor in St. Louis experienced its highest arithmetic mean in December of 2021. As depicted in Figure 3.15, the average Pb concentration for the year 2021 in St. Louis was 0.006 $\mu g/m^3$. According to the graph, it seems that the Blair Street Air Quality Monitor located in St. Louis recorded its highest arithmetic mean in May of 2022. As shown in Figure 3.16, the annual average Pb concentration for the year 2022 in St. Louis was 0.007 $\mu g/m^3$. It appears that the highest concentration of Pb was recorded in December for both the years 2020 and 2021, while it peaked in May for the year 2022, as per the data.

The presence of Pb in the air is primarily attributed to motor vehicles and industrial activities (27).

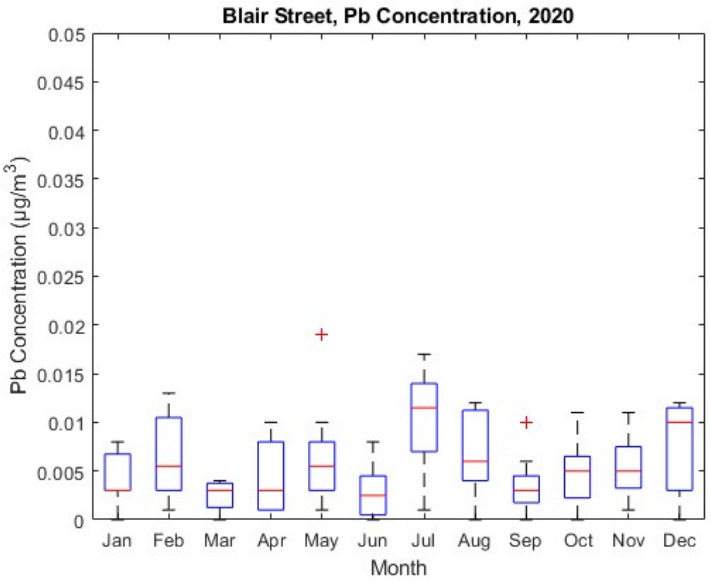

Figure 3.14 The graph of Pb concentration in St. Louis in 2020.

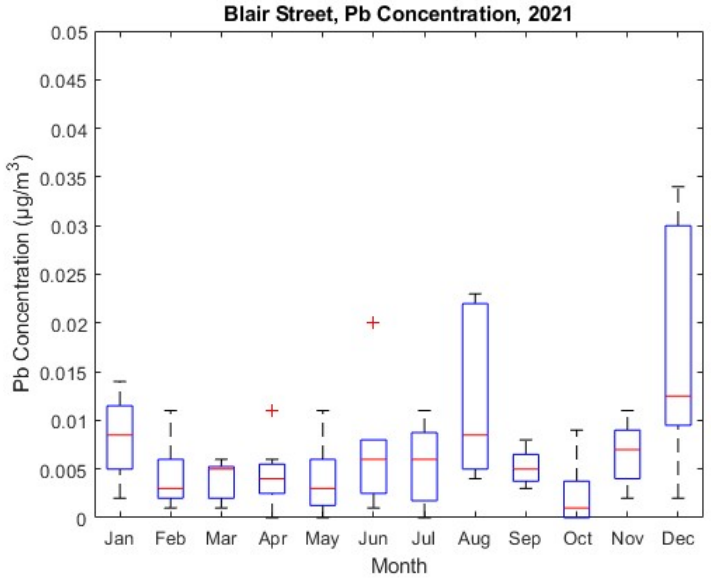

Figure 3.15 The graph of Pb concentration in St. Louis in 2021.

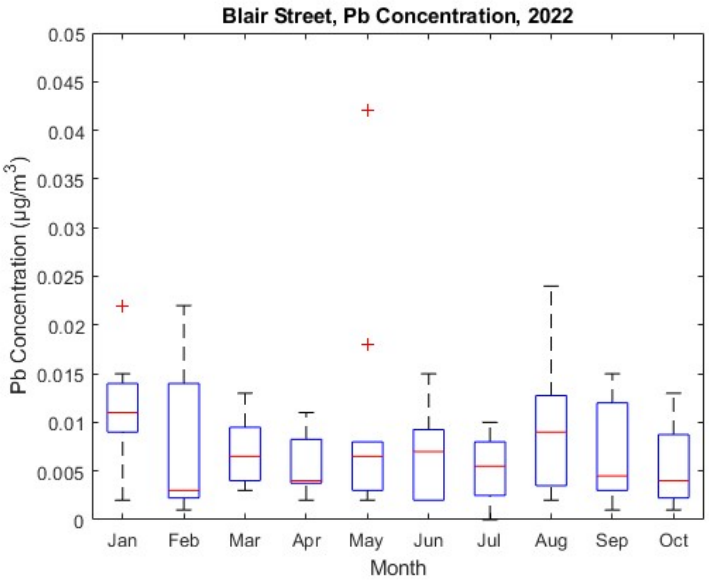

Figure 3.16 The graph of Pb concentration in St. Louis in 2022.

3.6. SULFUR DIOXIDE CONCENTRATION

Based on the graph, it can be observed that the Blair Street Air Quality Monitor in St. Louis recorded its highest arithmetic mean in September 2020. As shown in Figure 3.17, the annual average sulfur dioxide (SO_2) concentration in St. Louis for the year 2020 was 0.496 ppb. It is noteworthy that the annual average SO_2 concentration, 1-hour maximum daily concentration for over three years average primary standard is 75 ppb, according to the EPA National Ambient Air Quality Standards. Based on the graph, it can be observed that the Blair Street Air Quality Monitor in St. Louis recorded its highest arithmetic mean in September 2021. As depicted in Figure 3.18, the annual average SO_2 concentration in St. Louis for the year 2021 was 0.577 ppb. Based on the graph, it can be observed that the Blair Street Air Quality Monitor in St. Louis recorded its highest arithmetic mean in September 2022. As depicted in Figure 3.19, the annual average SO_2

concentration in St. Louis for the year 2022 was 0.627 ppb. According to a study, it has been generally concluded that the concentration of SO_2 reaches its peak in the month of September in the years 2020, 2021, and 2022. Industrial operations and the burning of fossil fuels are the major contributors to the release of SO_2 gas into the atmosphere (28). In addition, the study also revealed that an increase in the concentration of SO_2 in the air is caused by celebrations and fireworks on the Fourth of July.

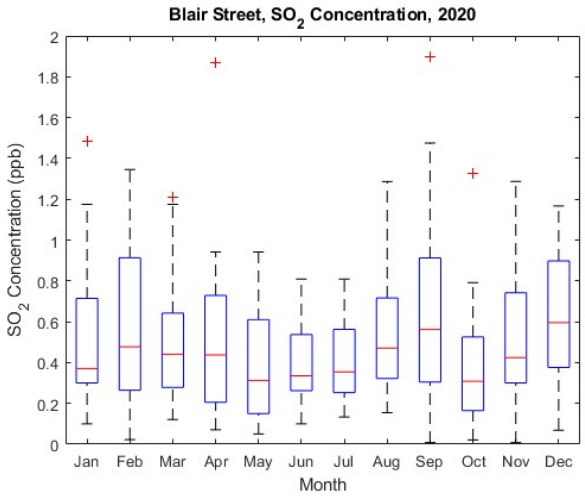

Figure 3.17 The graph of SO_2 concentration in St. Louis in 2020.

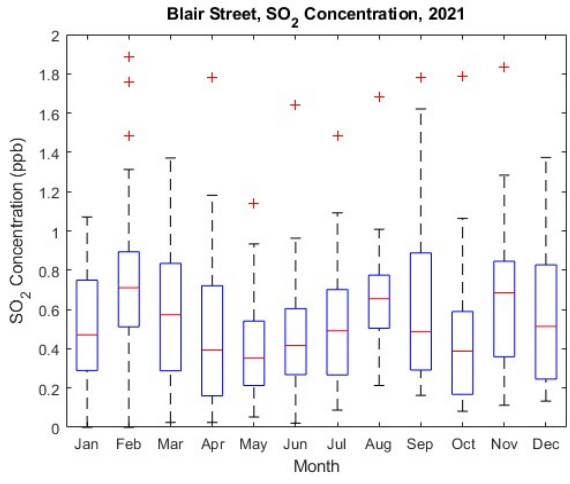

Figure 3.18 The graph of SO_2 concentration in St. Louis in 2021.

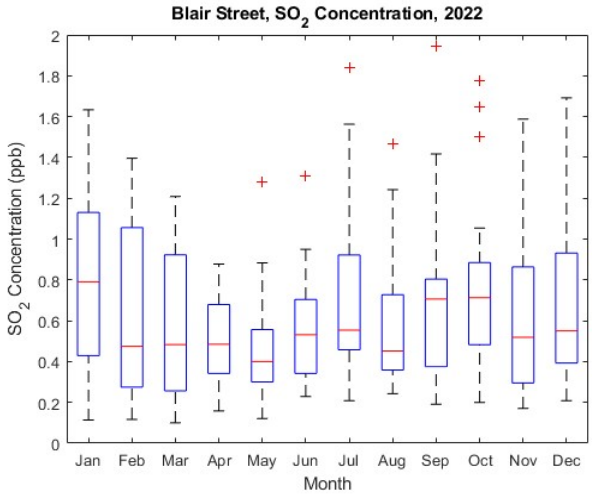

Figure 3.19 The graph of SO_2 concentration in St. Louis in 2022.

3.7. OZONE CONCENTRATION

Based on the graph, it shows that the Blair Street Air Quality Monitor in St. Louis is the only station where ozone (O_3) measurement is carried out, and it recorded its highest arithmetic mean in June. Further, Figure 3.20 indicates that the annual average O_3 concentration for 2020 in St. Louis is 0.0248 ppm. It's worth noting that the EPA National Ambient Air Quality Standards set the annual O_3 average at 0.070 ppm over eight hours. Based on the graph, it shows that the Blair Street Air Quality Monitor in St. Louis is the only station where O_3 measurement is carried out, and it recorded its highest arithmetic mean in April. Further, Figure 3.21 indicates that the annual average O_3 concentration for 2021 in St. Louis is 0.0275 ppm. Based on the graph, it shows that the Blair Street Air Quality Monitor in St. Louis is the only station where O_3 measurement is carried out, and it recorded its highest arithmetic mean in June. Further, Figure 3.22 indicates that the annual average O_3 concentration for 2022 in St. Louis is 0.0277 ppm. It has been reported that the highest concentration of O_3 for the years 2020 and 2022 was in June, while for the

year 2021, the highest concentration was in April. The increase in O_3 concentration is attributed to the chemical reaction between nitrogen oxides (NO_x) and volatile organic compounds (VOCs) emitted by traffic and industry, when exposed to sunlight. This process leads to the formation of O_3 in the atmosphere, as noted in source (29).

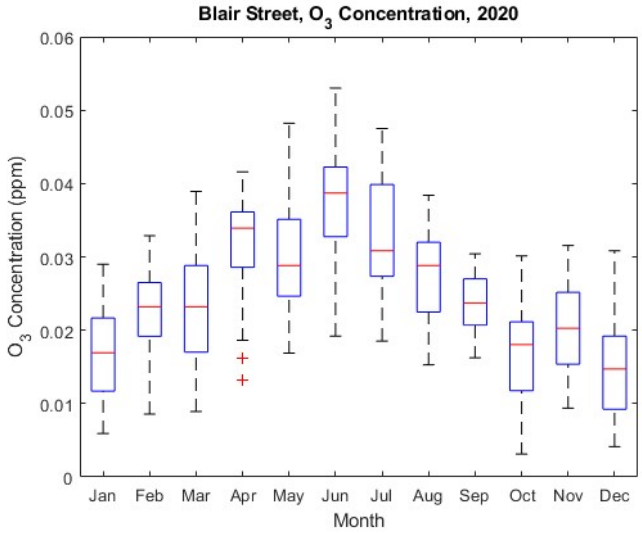

Figure 3.20 The graph of O_3 concentration in St. Louis in 2020.

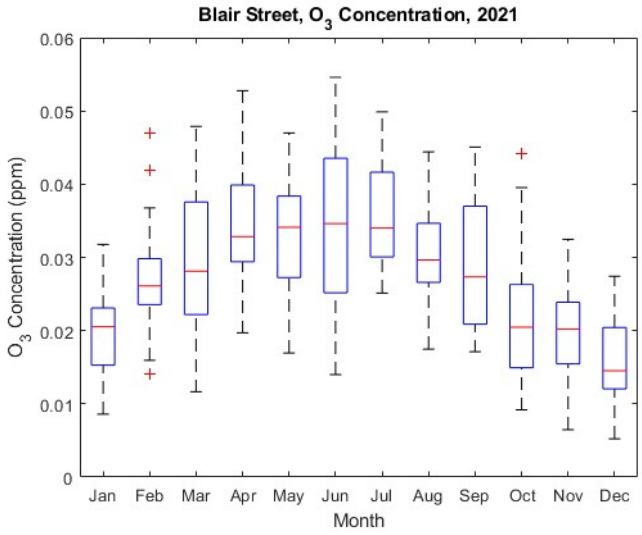

Figure 3.21 The graph of O_3 concentration in St. Louis in 2021.

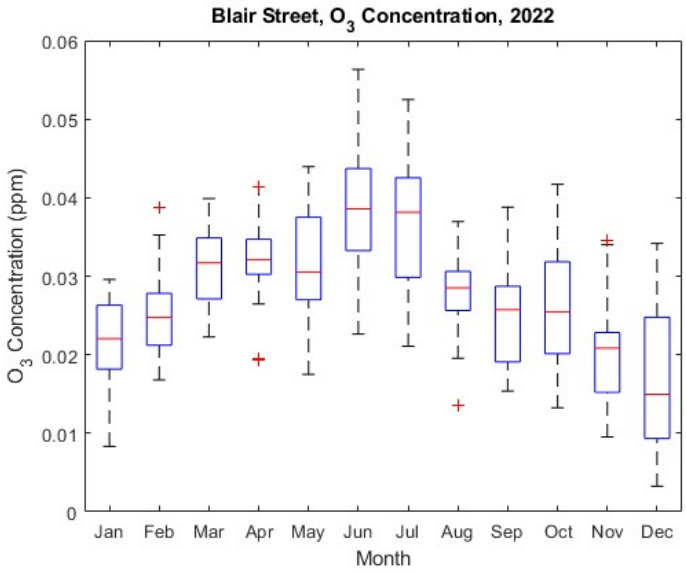

Figure 3.22 The graph of O_3 concentration in St. Louis in 2022.

4. USING HYSPLIT TO UNDERSTAND THE ORIGIN AND TRANSPORT OF AIR POLLUTANTS IN ST. LOUIS

4.1. BACKWARD TRAJECTORY, FORWARD TRAJECTORY AND CLUSTER ANALYSIS IN ST. LOUIS FOR 2020

St. Louis air quality monitor's arithmetic means reached its highest value in July 2020, according to all available data for $PM_{2.5}$ concentration. In July 2020, an analysis was carried out during the period when $PM_{2.5}$ concentration levels were at their highest. The analysis included generating forward and backward trajectory, as well as cluster analysis, which were conducted from July 3, 2020, to July 8, 2020. The objective of the study was to identify the sources and paths of air pollutants in St. Louis region. This type of analysis is essential in air pollution research.

As part of the analysis conducted from July 3, 2020, to July 8, 2020, a forward trajectory, backward trajectory, and cluster analysis were generated. Figure 4.1 (a) displays the number of backward trajectories identified during this period. According to TSV, a total of three clusters were found, with 21 backward trajectories identified. One of the trajectories, followed by 29 % of the clusters, originated from a location in Lake Michigan and traveled through Michigan, Wisconsin, and Illinois before reaching St. Louis. Another trajectory, followed by 48 % of the clusters, started from a location in Canada near the United States border and traveled through Minnesota, Wisconsin, and Illinois before reaching St. Louis. The last trajectory, followed by 24 % of the clusters, began in the Gulf of Mexico and traveled through Texas and Oklahoma before reaching St. Louis.

Figure 4.1 (b) displays the number of forward trajectories identified between July 3, 2020, and July 8, 2020. According to TSV, a total of two clusters were found, with 21

forward trajectories identified during this period. One of the trajectories, followed by 33 % of the clusters, began in St. Louis, traveled through Illinois and Lake Michigan, and then moved to Canada. The last trajectory, followed by 67 % of the clusters, started from St. Louis, moved through Kansas, Nebraska, Iowa, and traveled to Minnesota before moving to Wisconsin. The information regarding the number of trajectories, percentage of clusters, starting points, and directions between July 3, 2020, and July 8, 2020, is provided in Table 4.1.

Table 4.1 The number of trajectories, percentage of clusters, starting points and directions between July 3, 2020 and July 8, 2020.

Dates	Type of trajectories	Number of trajectories	Percentile of clusters	Starting location	Directions
July 3, 2020 – July 8, 2020	Backward trajectory	3	29 %	Lake Michigan	the northern direction
			48 %	Canada	the northwestern direction
			24 %	the Gulf of Mexico	the southern direction
	Forward trajectory	2	33 %	St. Louis	the northwestern direction
			67 %		the northwestern direction

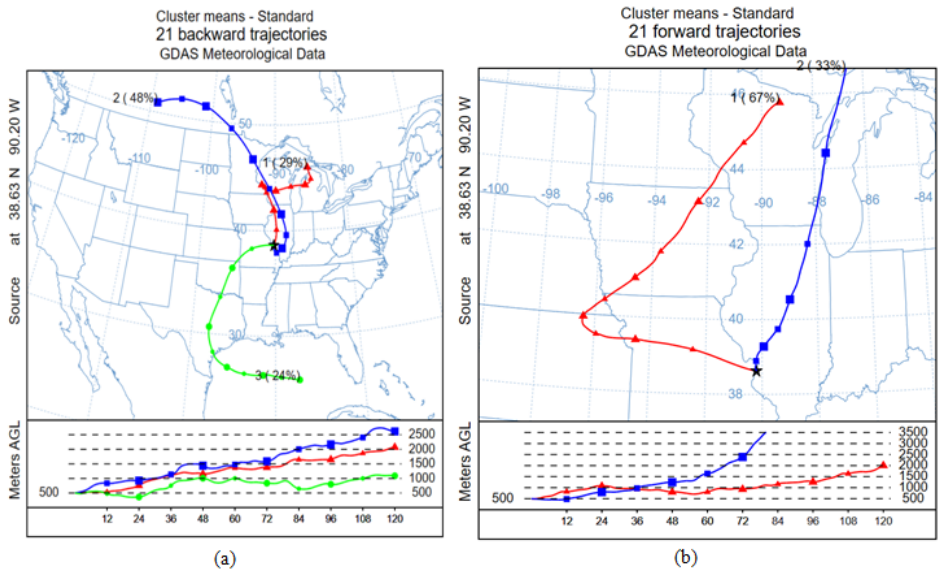

Figure 4.1 The number of trajectories between July 3, 2020 and July 8, 2020 (a) backward trajectory (b) forward trajectory.

- **HYSPLIT forward trajectory matrix analysis for 2020;**

Figure 4.2 shows the HYSPLIT forward trajectory matrix analysis that was created by selecting July 3, 2020, which was one of the days with the highest concentrations of $PM_{2.5}$ at 500 m above ground level. The analysis revealed that the pollutants moved away from the source area in the northwest, west, and northeast directions. The purpose of the HYSPLIT forward trajectory matrix analysis is to track the movement of air mass in the atmosphere and monitor air pollution. The results obtained from this analysis can be used to predict the future movement of atmospheric transport and evaluate these predictions under various scenarios, which is highly beneficial when it comes to understanding and addressing air pollution.

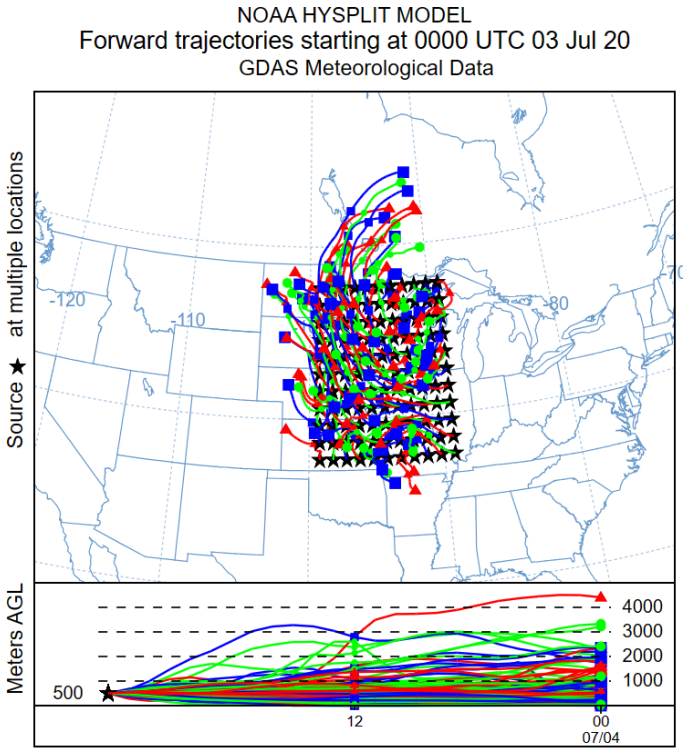

Figure 4.2 HYSPLIT forward trajectory matrix on July 4, 2020.

4.2. FORWARD TRAJECTORY, BACKWARD TRAJECTORY AND CLUSTER ANALYSIS IN ST. LOUIS FOR 2021

According to all available data for $PM_{2.5}$ concentration, the arithmetic means of St. Louis air quality monitors reached their highest value in July 2021. To investigate this, an analysis was conducted during the period with the highest concentration of $PM_{2.5}$. The analysis dates were July 3, 2021, to July 8, 2021, and involved generating forward trajectory, backward trajectory, and cluster analysis.

Figure 4.3 (a) displays the number of backward trajectories identified during this period. According to TSV, a total of three clusters were found, with 21 backward trajectories identified. The number of backward trajectories in the time span showed three clusters. One of the trajectories, followed by 43 % of the clusters, started from a location in Canada and traveled to St. Louis from the northern United States. Another trajectory, followed by 43 % of the clusters, began in the Gulf of Hudson, traveled through the north of Canada, and reached St. Louis. The last trajectory, followed by 14% of the clusters, started from northwestern Indiana, passed through Kentucky and Tennessee, turned in the northwestern direction, and found a pathway through Alabama and Tennessee before reaching St. Louis.

Figure 4.3 (b) displays the number of forward trajectories identified between July 3, 2021, and July 8, 2021. According to TSV, a total of two clusters were found, with 21 forward trajectories identified during this period. The number of forward trajectories in the time span showed two clusters. One of the trajectories, followed by 76 % of the clusters, started from St. Louis, moved through Illinois, Indiana, Ohio, and Pennsylvania from a northeastern direction, and found a pathway to Connecticut through Massachusetts to near northeastern Massachusetts' coastline in the Atlantic Ocean. The last trajectory, followed

by 24 % of the clusters, started from St. Louis, moved through Illinois, Indiana, Ohio, Pennsylvania, New York to Maine, and found a pathway through the northeastern Canadian coastline to the Atlantic Ocean near Greenland. The information regarding the number of trajectories, percentage of clusters, starting points, and directions between July 3, 2021, and July 8, 2021, is provided in Table 4.2.

Table 4.2 The number of trajectories, percentage of clusters, starting points and directions between July 3, 2021 and July 8, 2021.

Dates	Type of trajectories	Number of trajectories	Percentile of clusters	Starting location	Directions
July 3, 2021 – July 8, 2021	Backward trajectory	3	43 %	Canada	the northern direction
			43 %	the Gulf of Hudson	the northern direction
			14 %	Indiana	the southwestern direction
	Forward trajectory	2	76 %	St. Louis	the northwestern direction
			24 %		the northwestern direction

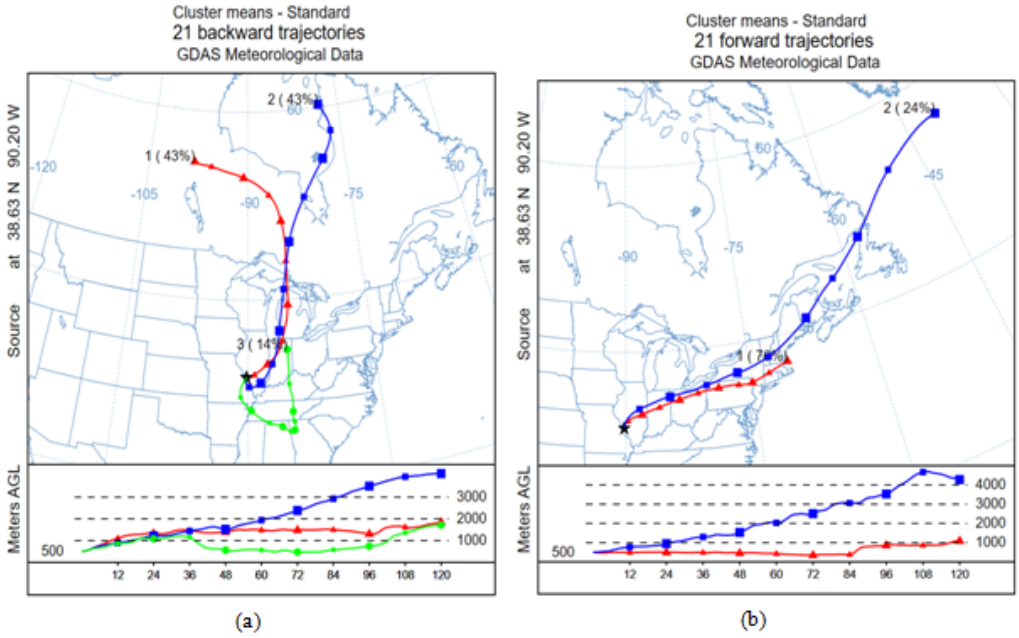

Figure 4.3 The number of trajectories between July 3, 2021 and July 8, 2021 (a) backward trajectory (b) forward trajectory.

- **HYSPLIT forward trajectory matrix analysis for 2021;**

Figure 4.4 displays the HYSPLIT forward trajectory matrix analysis, which was conducted by selecting July 4, 2021, one of the days with the highest concentrations of $PM_{2.5}$ at 500 m above ground level. The analysis revealed that the pollutants moved away from the source area in the northeast and east directions.

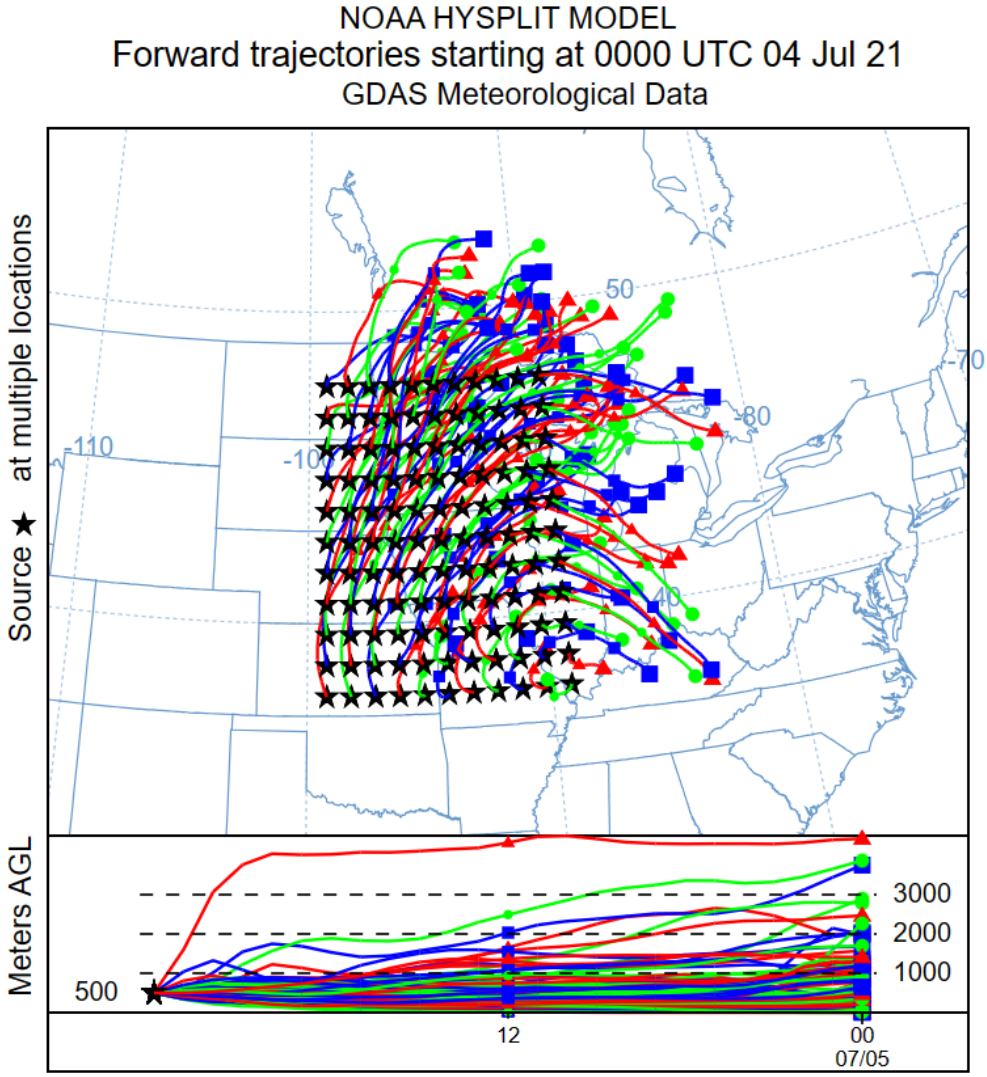

Figure 4.4 HYSPLIT forward trajectory matrix on July 4, 2021.

4.3. FORWARD TRAJECTORY, BACKWARD TRAJECTORY AND CLUSTER ANALYSIS IN ST. LOUIS FOR 2022

It has been reported that St. Louis air quality monitor recorded its highest $PM_{2.5}$ concentration in June 2022, based on the available data. In response to this, one analyses were conducted from June 12, 2022 to June 17, 2022 to investigate the origins and paths of air pollutants in the region. These analyses involved generating forward and backward trajectory analyses, as well as cluster analysis. Such studies play a crucial role in air pollution research and management.

As part of the analysis conducted from June 12, 2022 to June 17, 2022, a number of backward trajectories were generated, along with cluster analysis. Figure 4.5 (a) shows the number of backward trajectories during this time span. According to TSV, the analysis revealed three clusters, with a total of 21 backward trajectories. Specifically, the backward trajectories were divided into three clusters. The first trajectory was followed by 24 % of the clusters and started from somewhere in Nebraska, Kansas, Missouri, Arkansas, before returning to St. Louis. The second trajectory was followed by 43 % of the clusters and started from somewhere near the Cayman Islands in the Caribbean Sea, traversed through Mexico, Gulf of Mexico, and Texas, before reaching St. Louis. The third trajectory was followed by 33 % of the clusters and started from somewhere near the Dominican Republic in the Caribbean Sea, traversed through Mexico, Gulf of Mexico, and Texas, before reaching St. Louis.

Figure 4.5 (b) displays the number of forward trajectories generated between June 12, 2022 to June 17, 2022, as part of the analysis. According to TSV, the analysis revealed two clusters, with a total of 18 forward trajectories. The forward trajectories were divided into two clusters. The first trajectory was followed by 72 % of the clusters and started from

St. Louis, traversed through Illinois, Indiana, Ohio, Pennsylvania, and New York, and then moved to Canada's Gulf of Saint Lawrence. The second trajectory was followed by 28 % of the clusters and started from St. Louis, moved through Illinois, Canada, the Labrador Sea, and Greenland, Iceland, before moving near Norway in the North Sea. The information regarding the number of trajectories, percentage of clusters, starting points, and directions between June 12, 2022, and June 17, 2022, is provided in Table 4.3.

Table 4.3 The number of trajectories, percentage of clusters, starting points and directions between June 12, 2022 and June 17, 2022.

Dates	Type of trajectories	Number of trajectories	Percentile of clusters	Starting location	Directions
June 12, 2022 – June 17, 2022	Backward trajectory	3	24 %	Nebraska	the southern direction
			43 %	near Caman Island in Caribbean Sea	the southern direction
			33 %	near Dominic Republic in Caribbean Sea	the southern direction
	Forward trajectory	2	72 %	St. Louis	the northwestern direction
			28 %		the northwestern direction

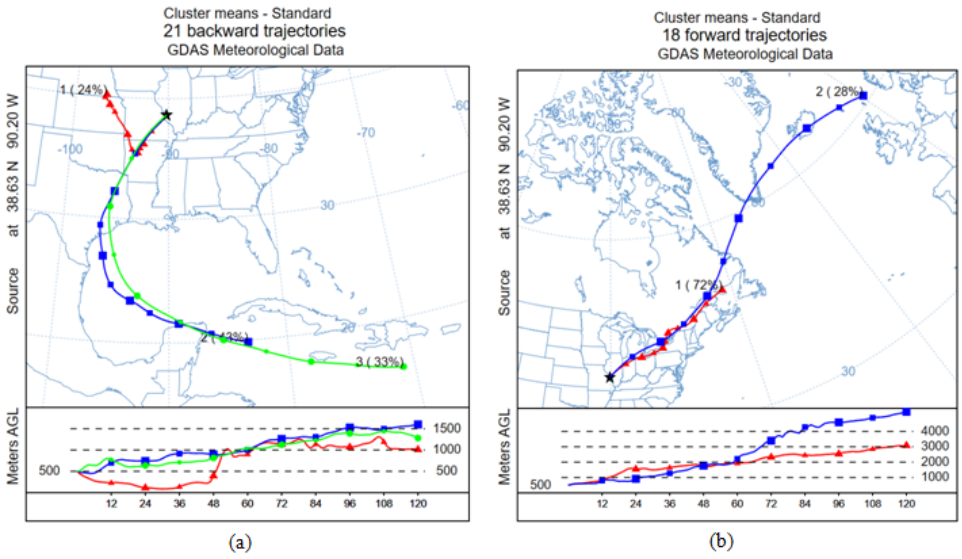

Figure 4.5 The number of trajectories between June 12, 2022 and June 17, 2022 (a) backward trajectory (b) forward trajectory.

- **HYSPLIT forward trajectory matrix analysis for 2022;**

Figure 4.6 illustrates the results of the HYSPLIT forward trajectory matrix analysis, which was conducted on June 15, 2022. This analysis was based on the $PM_{2.5}$ concentrations at an altitude of 500 m above the ground. The matrix generated by the HYSPLIT model shows that the pollutants moved away from the source area in the northeast and east directions.

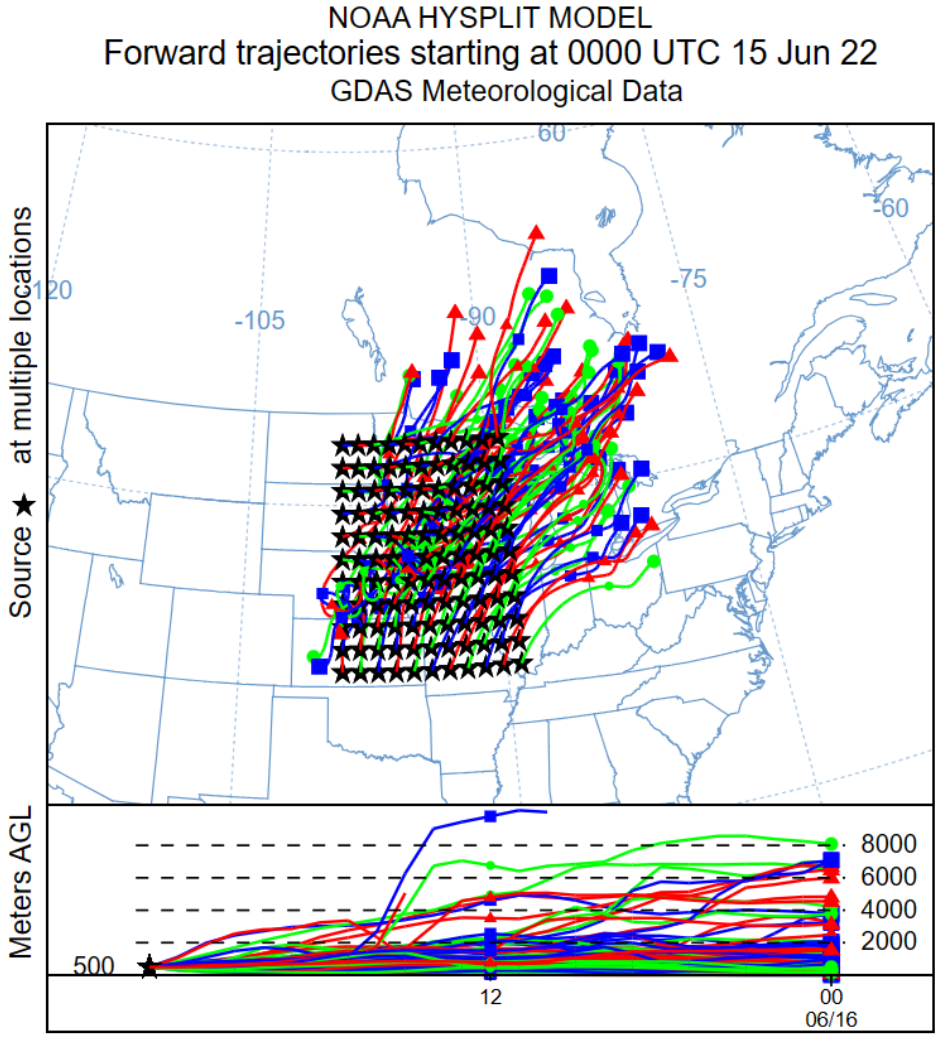

Figure 4.6 HYSPLIT forward trajectory matrix on June 15, 2022.

5. CONCLUSION AND FUTURE WORK

5.1. CONCLUSION

In this work, one of the air transport and dispersion models, HYSPLIT, was studied. The first part of the research involved examining monthly and seasonal air mass movements for the years 2020, 2021, and 2022. The results showed that each year had distinct starting points and trajectories. Furthermore, cluster analyses were conducted using different percentage distributions, which revealed that the contaminants followed various paths before reaching St. Louis.

The second part of this research focused on the analysis of air pollutants in St. Louis, using data from five EPA air quality monitors in the region for the years 2020, 2021, and 2022. The analysis indicated that the concentration of $PM_{2.5}$ reached its highest values during the summer months for all three years but was still below the EPA annual primary and secondary standards. The elevated concentrations of $PM_{2.5}$ and SO_2 were found to be caused by the usage of fireworks during the Fourth of July celebrations, as the release of particles into the air contributed to an increase in particulate matter concentration. On the other hand, the CO concentration reached its highest values during the autumn season for the years 2021 and 2022, while it peaked in the winter season in 2020, but still below the EPA National Ambient Air Quality Standards. The main contributors to increased concentrations of CO in the atmosphere were heating, motor vehicles, and industry. Furthermore, the NO_2 concentration reached its highest values in the spring season for 2021, while it peaked in the winter season for both 2020 and 2022, but still below the EPA National Ambient Air Quality Standards. The main contributors to increased

concentrations of NO_2 and NO in the atmosphere were vehicle emissions and industrial operations in manufacturing facilities. The Pb concentration reached its highest values during the winter season for the years 2020 and 2021, while it peaked in the spring season for 2022, but still below the EPA National Ambient Air Quality Standards. The main sources of Pb in the air were motor vehicles and industrial operations. Additionally, the sulfur dioxide concentration reached its highest values during the autumn season for all three years, but still below the EPA National Ambient Air Quality Standards. Industrial activities and the burning of fossil fuels were identified as the main contributors to increased concentrations of sulfur dioxide gas in the atmosphere. Finally, it was found that the O_3 concentration reached its highest values during the summer season for 2020 and 2022, while it peaked in the spring season for 2021, but still below the EPA National Ambient Air Quality Standards. Nitrogen oxides (NO_x) and volatile organic compounds (VOCs) released from traffic and industry were found to react chemically and increase the concentration of O_3 in the air when exposed to sunlight.

In the third part of this research, backward and forward trajectory analysis, as well as cluster analysis, were performed using the HYSPLIT program to determine the origin and destination of PM pollutants in 2020, 2021, and 2022. The dates with the highest values were selected for this analysis. The backward trajectory analysis showed that pollutants often traveled from the North and South of the United States to St. Louis in all three years, while they were observed moving forward from St. Louis to the North of the United States. Therefore, the results suggest that pollutants mainly enter St. Louis region from the southeast and northwest, as indicated by the backward trajectory analysis. In addition, pollutants typically move in a northeasterly direction away from St. Louis region.

5.2. FUTURE WORK

Future research could focus on conducting a comprehensive analysis of pollutants entering and leaving St. Louis region to determine the sources of specific pollutants, their distribution in the atmosphere, and their effects on the environment. This analysis would require a comprehensive inventory of all pollutants from industrial, transportation, and residential sources in the area where the pollutant enters St. Louis or from all industrial, transportation, and residential sources in St. Louis area. It is important to ensure accurate data collection and coordination with local authorities to achieve an efficient inventory process. In addition, field studies should be conducted to examine the environmental effects of pollutants from different parts of St. Louis region. Samples should be taken from these regions, and these samples should be analyzed to analyze in detail the effects of regional pollutants on the environment and human health in the analysis of air quality in St. Louis region.

It is possible to conduct laboratory tests and epidemiological studies to investigate the effects of pollutants on the health of St. Louis residents. The results of these studies can be used to prepare a detailed report on the impact of air pollutants on human health. It is important to conduct further research to understand the connection between pollutant transportation, atmospheric dispersion, meteorological factors, and topography. Meteorological data can be compared to analyze atmospheric transport and dispersion, while precise information about elevations can be obtained by analyzing the topography of St. Louis region. The HYSPLIT modeling program can be utilized to simulate various scenarios for detailed analysis and comparison of data. Additionally, conducting detailed

examinations of air quality monitoring stations and potentially relocating or increasing the number of stations can provide valuable information. By incorporating all of this data, a comprehensive analysis can be conducted to make more informed decisions regarding the effects of air pollution.

In order to gain insight into the transport of air pollution from the poles to the equator and the characteristics of wind movements (30), it is recommended to conduct a Polar Wind Analysis study for St. Louis. This study can provide detailed information on the impact of polar winds on air pollution and air quality. By conducting a thorough analysis of polar winds, it is possible to identify any issues related to air pollution and take the necessary measures to address them. As most of the air coming into St. Louis comes from the north, this study can be particularly useful in understanding the impact of polar winds on air quality in the area. The results of this analysis can provide valuable insights and inform decision-making related to improving air quality in St. Louis.

REFERENCES

[1] P. J. Samson, “Atmospheric Transport and Dispersion of Air Pollutants Associated with Vehicular Emissions. Air Pollution, the Automobile, and Public Health,” Watson AY, Bates RR, Kennedy D, editors. Air Pollution, the Automobile, and Public Health. Washington (DC): National Academies Press (US); 1988. Available: https://www.ncbi.nlm.nih.gov/books/NBK218142/?report=printable

[2] M. Hutchinson, H. Oh, W.-H. Chen, “A review of source term estimation methods for atmospheric dispersion events using static or mobile sensors,” Information Fusion, Vol. 36, pp. 130-148, July 2017. Available: http://dx.doi.org/10.1016/j.inffus.2016.11.010.

[3] M. Kulmala, L. Laakso, K. E. J. Lehtinen, I. Riipinen, M. Dal Maso, T. Anttila, V.-M. Kerminen, U. H˜orrak,M. Vana, and H. Tammet, “Initial steps of aerosol growth,” ,” Atmospheric Chemistry and Physics, Vol.4, Issue 11/12, pp. 2553–2560, 15 Dec., 2004. Available: https://doi.org/10.5194/acp-4-2553-2004.

[4] A. Aili, J. Abuduwaili, H. Xu, X. Zhao, and X. Liu, “A Cluster Analysis of Forward Trajectory to Identify the Transport Pathway of Salt-Dust Particles from Dried Bottom of Aral Sea, Central Asia,” Atmosphere. 12(6):764, 2021. Available: https://doi.org/10.3390/atmos12060764

[5] A. Ghorani-Azam, B. Riahi-Zanjani, M. Balali-Mood, “Effects of air pollution on human health and practical measures for prevention in Iran,” Journal of Research in Medical Sciences, 2016. Available: doi:10.4103/1735-1995.189646

[6] P.M. Mannucci, M. Franchini, “Health Effects of Ambient Air Pollution in Developing Countries,” International Journal of Environmental Research and Public Health, 2017. Available: doi:10.3390/ijerph14091048

[7] X. Jiang, X. Mei, D. Feng, “Air pollution and chronic airway diseases: what should people know and do?,” Journal of Thoracic Disease, 2015. Available: doi: 10.3978/j.issn.2072-1439.2015.11.50

[8] AirNow, AQI Technical Assistance Document, May 2020, Retrieved November 1, 2023, from https://www.airnow.gov/sites/default/files/2020-05/aqi-technical-assistance-document-sept2018.pdf

[9] M. Modi, V. R. P, L. A. SK, and Z. Hussain, "A Review on Theoretical Air Pollutants Dispersion Models," International Journal of Pharmaceutical, Chemical and Biological Sciences, IJPCBS 2013, 3(4), 1224-1230

[10] J.B. Johnson, "An Introduction to Atmospheric Pollutant Dispersion Modelling," 5th International Electronic Conference on Atmospheric Sciences, 16–31 July 2022, Virtual Conference. Available online: https://ecas2022.sciforum.net/.

[11] N.E. Daidzic, "On Atmospheric Lapse Rates," International Journal of Aiation, Aeronautics, and Aerospace, 6(4), 2019, Available: https://doi.org/10.15394/ijaaa.2019.1374

[12] A. F. Stein, R. R. Draxler, G. D. Rolph, B. J. B. Stunder, M. D. Cohen, and F. Ngan, "NOAA's HYSPLIT Atmospheric Transport and Dispersion Modeling System," American Meteorological Society, Vol. 96, April, 2015. Available: https://journals.ametsoc.org/view/journals/bams/96/12/bams-d-14-00110.1.xml?tab_body=supplementary-materials.

[13] B. E. Moroz, H. L. Beck, A. Bouville, and S. L. Simon, "Predictions of Dispersion and Deposition of Fallout from Nuclear Testing Using the NOAA-HYSPLIT Meteorological Model," Health Physics, Vol. 99, Issue 2, pp.252-269, Aug., 2010. Available: DOI: 10.1097/HP.0b013e3181b43697.

[14] F. Ngan, A. stein, and R. Draxler, "Inline Coupling of WRF–HYSPLIT: Model Development and Evaluation Using Tracer Experiments," Journal of Applied Meteorology and Climatology, Vol. 54, pp. 1162-1176, Feb., 2015. Available: DOI: 10.1175/JAMC-D-14-0247.1.

[15] M. Ni'am, I. S. Sitanggang, and D. E. Nuryanto, "Clustering of CO and CO_2 concentration from Sumatra peat fire haze using HYSPLIT and K-means algorithm," in IOP Conference Series: Earth and Environmental Science,Volume 54, The 3rdInternational Symposium on LAPAN-IPB Satellite For Food Security and Environmental Monitoring 2016, Bogor, Indonesia, 25–26 October 2016, Available: DOI 10.1088/1755-1315/54/1/012054.

[16] M. Rajasekhar, M. Devendra Kumar, T. Subbananthan, V.K. Srivastava, B.V. Apparao, V. Seshagiri Rao, and M.Y.S. Prasad, "Exhaust Dispersion Analysis from Large Solid Propellant Rocket Motor Firing Using Hysplit Model Over Satish Dhawan Space Centre (Sdsc Shar)," in Indo-US Conference-cum-Workshop on "Air Quality and Climate Research," ASCI Hyderabad, India, March 2011.

[17] L. Su, Z. Yuanb, J.C.H. Fung, A. K.H. Lau, "A comparison of HYSPLIT backward trajectories generated from two GDAS datasets," Science of the Total Environment Vol. 506–507, pp. 527–537, 15 Feb., 2015. Available: http://dx.doi.org/10.1016/j.scitotenv.2014.11.072.

[18] O. Skrynyka, V. Voloshchuka, I. Budaka, and S. Bubinb, "Regional HYSPLIT simulation of atmospheric transport and deposition of the Chernobyl ^{137}Cs releases," Atmospheric Pollution Research Vol. 10, Issue 6, pp. 1953–1963, Nov. 2019. Available: https://doi.org/10.1016/j.apr.2019.09.001.

[19] L. Myles, W. R. Pendergrass, C. A. Vogel, A.Yerramilli, V. B. R. Dodla, H. P. Dasari, C.V. Srinivas, F. Tuluri, J. M. Baham, R. Hughes, C. Patrick, J. Young, and S. Swanier, "Evaluation Of PM2.5 Source Regions Over The Mississippi Gulf Coast Using WRF/HYSPLIT Modeling Approach," in 16th Conference on Air Pollution Meteorology, Joint Session 3, Air Pollution and Meteorological Modeling and Measurements in the Coastal Environment (Joint with the Committee on Coastal Environment), 20 Jan. 2010.

[20] D. M. Hondula, L. Sitka, R. E. Davis, D. B. Knight, S. D. Gawtry, M. L. Deaton, T. R. Lee, C. P. Normile, and P. J. Stengera, "A back-trajectory and air mass climatology for the Northern Shenandoah Valley, USA," International Journal of Climatology, Vol. 30, Issue 4, pp. 569-581, 30 March 2010. Available: https://doi.org/10.1002/joc.1896.

[21] Q. Wang,T. Zhao, R. Wang, and L. Zhang, "Backward Trajectory and Multifractal Analysis of Air Pollution in Zhengzhou Region of China," Mathematical Problems in Engineering, Vol. 2022, pp. 1-17, 13 Jan., 2022. Available: https://doi.org/10.1155/2022/2226565.

[22] R. Draxler, B. Stunder, G. Rolph, A. Stein, A. Taylor, S. Zinn, C. Loughner, and A. Crawford, "HYSPLIT User's Guide," National Oceanic and Atmospheric Administration, Version 5.2 - Last Revision: Jan., 2022. Available: https://www.arl.noaa.gov/documents/reports/hysplit_user_guide.pdf.

[23] G. S. Thomas, “"Observations of the tapered element oscillating microbalance as compared to a gravimetric method for particulate matter measurement," 2008, Graduate Theses, Dissertations, and Problem Reports. 1990. Available: https://researchrepository.wvu.edu/etd/1990.

[24] D. Massey, A. Kulshrestha, J. Masih, and A. Taneja, “Seasonal trends of PM10, PM5.0, PM2.5 & PM1.0 in indoor and outdoor environments of residential homes located in North-Central India.” Building and Environment, 47, 223-231, 2012. Available: https://doi.org/10.1016/j.buildenv.2011.07.018

[25] Y. Té, P. Jeseck, B. Franco, E. Mahieu, N. Jones, C. Paton-Walsh, D.W.T. Griffith, R.R. Buchholz, J. Hadji-Lazaro, D. Hurtmans, and C. Janssen, “Seasonal variability of surface and column carbon monoxide over the megacity Paris, high-altitude Jungfraujoch and Southern Hemispheric Wollongong stations.” Atmos. Chem. Phys., 16, 10911–10925, 2016. Available: https://doi.org/10.5194/acp-16-10911-2016, 2016.

[26] D. Alejo, M.C. Morales, J.B. de la Torre, R. Grau, L. Bencs, R. Van Grieken, P. Van Espen, D. Sosa, and V. Nuñez, “Seasonal trends of atmospheric nitrogen dioxide and sulfur dioxide over North Santa Clara, Cuba.” Environmental monitoring and assessment, 185(7), 6023–6033, 2013. Available: doi: https://doi.org/10.1007/s10661-012-3003-4

[27] Texas Commission on Environmental Quality (TCEQ). (n.d.). State Implementation Plan (SIP) for Lead. Retrieved from https://www.tceq.texas.gov/airquality/sip/criteria-pollutants/sip-lead

[28] B. Zhang, “The Effect of Aerosols to Climate Change and Society. Journal of Geoscience and Environment Protection,” Journal of Geoscience and Environment Protection, 8, 55-78, 2020. Available: doi: https://doi.org/10.4236/gep.2020.88006

[29] J.J. Zhang, Y. Wei, and Z. Fang “Ozone Pollution: A Major Health Hazard Worldwide.” Front. Immunol. 10:2518, 2019. Available: doi: 10.3389/fimmu.2019.02518

[30] L.A. Barrie, “Arctic air pollution: An overview of current knowledge’” Atmospheric Environment (1967), Vol. 20, Issue 4 pp. 643-663, 1986, Available: https://doi.org/10.1016/0004-6981(86)90180-0

VITA

Ahmet Tolga Odabaşı was born in Istanbul, Türkiye. He earned his Bachelor of Engineering degree in Environmental Engineering from Yıldız Technical University. Subsequently, he commenced his master's degree program in Environmental Engineering at Missouri University of Science and Technology, where his research focused on Atmospheric Dispersion of Hazardous Aerosols. Throughout his academic journey, he received sponsorship from the Ministry of National Education, Republic of Türkiye, and was under the guidance and supervision of Dr. Yang Wang. Ahmet Tolga Odabaşı received his Master of Science degree in Environmental Engineering in December 2023 from Missouri University of Science and Technology, located in Rolla, Missouri, USA.